

The most metal-rich damped Lyman α systems at $z \gtrsim 1.5$ I: The Data

Trystyn A. M. Berg

Department of Physics and Astronomy, University of Victoria, Victoria, British Columbia, V8P 1A1, Canada.

trystynb@uvic.ca

Marcel Neeleman

Department of Physics and Center for Astrophysics and Space Sciences, UCSD, La Jolla, CA 92093, USA.

J. Xavier Prochaska

Department of Astronomy and Astrophysics, University of California, Santa Cruz, Santa Cruz, CA, 95064, USA.

Sara L. Ellison

Department of Physics and Astronomy, University of Victoria, Victoria, British Columbia, V8P 1A1, Canada.

and

Arthur M. Wolfe¹

Department of Physics and Center for Astrophysics and Space Sciences, UCSD, La Jolla, CA 92093, USA.

ABSTRACT

We present HIRES observations for 31 damped Lyman α systems, selected on the basis of their large metal column densities from previous, lower resolution data. The measured metal column densities for Fe, Zn, S, Si, Cr, Mn, and Ni are provided for these 31 systems. Combined with previously observed large metal column density damped Lyman α systems, we present a sample of 44 damped Lyman α systems observed with high resolution spectrographs ($R \sim 30000$). These damped Lyman α systems probe the most chemically evolved systems at redshifts greater than 1.5. We discuss the context of our sample with the general damped Lyman α population, demonstrating that we are probing the top 10% of metal column densities with our sample. In a companion paper, we will present an analysis of the sample's elemental abundances in the context of galactic chemical enrichment.

Subject headings: Galaxies; Astrophysical Data

1. Introduction

Damped Lyman α systems (DLAs) are quasar absorption line systems with the largest neutral hydrogen column densities ($\log N(\text{HI}) \geq 20.3$; Wolfe et al. 1986) and are particularly useful to study the evolution of galaxies from redshifts $z \sim 0$ –5. These sight-lines through gas-rich galaxies (Wolfe et al. 1995) contain information on the kinematics (Prochaska & Wolfe 1997; Haehnelt et al. 1998; Ledoux et al. 2006; Neeleman et al. 2013; Christensen et al. 2014), chemistry (Pettini et al. 1990; Lu et al. 1996; Prochaska et al. 2001b; Dessauges-Zavadsky et al. 2004, 2006a; Ellison et al. 2010a; Penprase et al. 2010; Ellison et al. 2011; Battisti et al. 2012), and physical conditions (Ledoux et al. 2003; Srianand et al. 2005, 2008; York et al. 2007; Milutinovic et al. 2010; Tumlinson et al. 2010; Ellison et al. 2012; Fynbo et al. 2013; Krogager et al. 2013a; Kanekar et al. 2014) of the constituent interstellar gas. Coupled with high resolution spectrographs, observations of DLAs can provide accurate chemical compositions that allow us to understand what processes are taking place within the absorbing galaxies (e.g. Pettini et al. 1994, 1997, 2000; Ellison et al. 2001; Ledoux et al. 2002; Prochaska & Wolfe 2002; Lopez & Ellison 2003; Akerman et al. 2005).

Previous work has demonstrated that DLAs span a wide range in metallicity where the majority of DLAs have metallicities similar to those seen in halo stars and metal-poor disk stars (e.g. Pettini et al. 1997; Rafelski et al. 2012). Recent work by Penprase et al. (2010); Cooke et al. (2011, 2014) has focussed on the extremely metal-poor end of the distribution to study the chemical enrichment of Population III stars and metal-poor dwarf galaxies. However, little work has examined the *most massive, chemically evolved* DLAs. Such studies would provide insight into dust formation (Pettini et al. 1997; Ledoux et al. 2002; Vladilo et al. 2011) and nucleosynthetic constraints (Ellison et al. 2001; Zafar et al. 2014a,b) within the first few Gyr of galaxy evolution. In Berg et al. (2013) we presented results on the first systematic search for boron in DLAs with large metal contents, as an example of the potential for exotic element studies at high redshifts in DLAs.

A class of DLAs with large metal column densities are known as metal-strong DLAs (MSDLAs). Inspired by the first detections of exotic elements (e.g. boron, chlorine, and germanium) in the sight-line towards the quasar FJ0812+3208 (Prochaska et al. 2003c), Herbert-Fort et al. (2006, HF06) defined a classification scheme identifying MSDLA candidates within the Sloan Digital Sky Survey (SDSS) DLA catalogues (Prochaska & Herbert-Fort 2004; Prochaska et al. 2005) based on the strength of the SiII and ZnII absorption lines. According to their scheme, MSDLAs require metal column densities of $\log N(\text{ZnII}) \geq 13.15$ or $\log N(\text{SiII}) \geq 15.95$. These limits in zinc and silicon

¹Deceased

column densities were subjectively chosen such that weak lines from rarely detected elements (such as boron, tin, and lead) could be observed in a typical high resolution spectrum purely due to the higher number of metal atoms along the sight-line. HF06 used follow-up ESI observations to evaluate the ability to correctly identify MSDLAs from SDSS equivalent widths and visual identification, while Kaplan et al. (2010) obtained $N(\text{HI})$ for a handful of systems to determine their metallicity. However, a large collection of MSDLAs does not currently exist and no follow-up work on MSDLAs has been published since Kaplan et al. (2010).

In this series of papers, we are interested in the metal enrichment of the most massive, metal-rich, star forming DLAs at $z \sim 2$. These DLAs probe the nucleosynthetic environments similar to the metal-rich disk stars (in particular the thin disk which spans from $-0.8 \leq [\text{Fe}/\text{H}] \leq 0.2$; Edvardsson et al. 1993), a regime that exceeds the metallicity of the typical DLA observed. In addition, because exotic elements (e.g. boron) have weak oscillator strengths and small abundances, the chemical evolution of these elements can also be studied in MSDLAs. In this paper, we present new data on the follow-up 31 candidate MSDLAs from the HF06 catalogue, adding to the 13 systems previously studied in the literature (HF06; Kaplan et al. 2010). We include a description of the high resolution spectroscopic observations and details of the abundance analysis used in Berg et al. (2013) and Berg et al. (in preparation; hereafter Paper II). In addition, we revisit the MSDLA criteria defined by HF06, and discuss its significance to our sample and its impact on studying chemical evolution at high redshifts. In Paper II we will present a full analysis of the our sample’s abundances in the context of local stellar populations to provide insights into the nucleosynthesis of galaxies in the first few Gyr of the universe.

2. cMSDLA Sample

2.1. Sample Selection

We have observed 31 DLAs, which were pre-selected by their *very strong* metal lines in SDSS spectra (as classified by HF06). Each of these 31 DLAs were targeted for one of three specific science cases: 1) to study the chemical enrichment of DLAs (Prochaska et al. 2003a), 2) for the measurement of C I (Jorgenson et al. 2010), or 3) the detection of $[\text{C II}] \lambda 158$ micron emission with ALMA. In all of these cases we require a relatively bright background quasar ($R \leq 19$). The last case also requires the MSDLA candidate to fall within the observing range of ALMA (i.e. $\delta \leq 15^\circ$), and the 158 micron line be shifted into an observing band of ALMA (i.e. $1.70 \leq z_{\text{abs}} \leq 2.04$). To increase the sample size, we supplemented this sample of DLAs with 13 additional high metal column density systems from the literature (HF06; Kaplan et al. 2010). These 13 DLAs were selected solely based on their high-metal content. As the total sample of 44 DLAs has been pre-selected on metal content such that there is a greater likelihood they meet the MSDLA criterion (HF06), we refer to this sample as the candidate MSDLA (hereafter referred to as the *cMSDLA sample*), which will provide an excellent sample of DLAs to study the chemistry of metal enriched environments at high

redshift.

2.2. Observation Details

The new 31 DLAs were observed with the High Resolution Spectrograph (HIRES; Vogt et al. 1994) on the Keck I telescope, spanning over several observing runs from 2005 to 2012. The 3-chip mosaic of MIT-LL 2048x4096 CCDs was used with either a 0.86" or 1.15" slit, resulting in a maximum full width at half maximum resolution of 6 and 8 km s⁻¹ respectively. All of the spectra were binned by two pixels in the spatial direction. However, for some observations the data were also binned by two in the spectral direction to reduce read noise per resolution element. This resulted in a pixel size of 2.8 km s⁻¹ instead of 1.4 km s⁻¹ for these observations. These high resolution spectra are necessary to resolve the entire kinematic structure of the metal absorption lines to derive accurate column densities and test whether the metal lines suffer from contamination or saturation. The sample of 31 new DLAs were observed over a span of 14 nights under a variety of different conditions. A journal of the observations is presented in Table 1.

The raw data were reduced using the `HIREDUX` routine, then extracted, coadded and continuum fit with `x_continuum`. These routines are all part of the publicly available `XIDL`² reduction package developed by J.X. Prochaska. Also shown in Table 1 is the typical range in the signal-to-noise ratio per pixel (S/N) for each of the observed DLAs redwards of the Ly- α absorption.

For the majority of the cMSDLAs in Table 1, HI column densities have been previously obtained from other observations with instruments such as the Echellette and Imaging Spectrometer (ESI; Sheinis et al. 2002) on the Keck II 10m telescope and the spectra from SDSS. Unfortunately for some cases, the Ly- α absorption line for absorbers with redshifts less than 2.2 fall below the wavelength coverage of either of these instruments, prompting observations of DLAs with redshifts below 2.2 using the blue channel spectrograph (BCS) on the MMT telescope (Kaplan et al. 2010). Even so, for 18 of the DLAs, no spectra with Ly- α coverage exist and we have to rely on direct measurements from the HIRES spectra. However the Ly- α line of a high column density absorber, such as a DLA, spreads over several orders of the HIRES spectrograph and therefore the placement of the continuum over these orders is not well-constrained. For this reason, and the difficulty of fluxing HIRES spectra (Suzuki et al. 2003), we give preference to N(HI) estimates made from ESI or BCS spectra where possible.

To test our determination of the HI column density for the cases where we were required to use the HIRES spectra (Section 3.1), we have followed-up 4 of the absorbers using the Kast spectrograph on the Shane 3m telescope. For these observations, we used the 830 line mm⁻¹ grism centered at ~ 3850 Å with a 2" slit. This resulted in a resolution of 0.63 Å per pixel. The journal of observations,

²<http://www.ucolick.org/~xavier/IDL/>

Table 1: QSO targets and observation details

QSO	R.A.	Dec.	z_{em}	Magnitude (R)	Decker	Binning	Observation date	Exposure time (s)	S/N pixel ⁻¹
J0008–0958	00:08:15.3	–09:58:54.0	1.95	18.3	C1	2x1	2010 September 02	15029	11 – 21
J0044+0018	00:44:39.3	+00:18:22.7	1.87	18.4	C1	2x1	2012 January 16	3600	2 – 12
J0058+0115	00:58:14.3	+01:15:30.2	2.50	17.4	C1	2x1	2005 October 26	14400	11 – 31
J0211+1241	02:11:29.16	+12:41:10.8	2.95	18.9	C1	2x1	2011 January 25	10200	3 – 10
J0233+0103	02:33:33.2	+01:03:33.1	2.06	18.5	C5	2x1	2012 January 16	3600	2 – 9
J0815+1037	08:15:19.0	+10:37:11.5	2.02	18.3	C1	2x1	2012 January 16	2237	2 – 3
J0927+1543	09:27:59.8	+15:43:21.8	1.80	18.8	C1	2x1	2011 January 25	5600	7 – 10
J0927+5823	09:27:08.8	+58:23:19.4	1.91	18.3	C1	2x1	2011 January 26	21600	11 – 20
J0958+0145	09:58:22.2	+01:45:24.2	1.96	17.9	C1	2x1	2012 January 16	3600	2 – 16
J1013+5615	10:13:36.4	+56:15:36.4	3.61	18.4	C1	2x1	2006 January 05	3600	8 – 12
J1024+0600	10:24:10.4	+06:00:13.8	2.13	18.7	C1	2x2	2012 April 15	1800	2 – 13
J1042+0628	10:42:13.5	+06:28:53.0	2.04	18.8	C1	2x2	2012 April 15	2400	6 – 12
J1049–0110	10:49:15.4	–01:10:38.1	2.12	17.8	C5	2x2	2006 January 04	4800	10 – 25
J1056+1208	10:56:48.7	+12:08:26.8	1.92	17.9	C1	2x1	2011 January 25	21300	10 – 24
J1106+1044	11:06:21.4	+10:44:32.6	1.86	19.0	C1	2x2	2012 April 15	2700	7 – 11
J1142+0701	11:42:44.9	+07:01:03.2	1.87	18.7	C1	2x1	2012 January 16	10200	4 – 8
J1155+0530	11:55:38.60	+05:30:50.6	3.48	18.1	C1	2x1	2005 April 14	7200	12 – 28
J1305+0924	13:05:42.8	+09:24:27.8	2.06	18.6	C1	2x2	2012 April 15	2400	5 – 12
J1310+5424	13:10:40.24	+54:24:49.6	1.93	18.5	C1	2x2	2005 March 17	10800	9 – 24
J1313+1441	13:31:41.2	+14:41:40.6	1.88	18.2	C1	2x1	2006 June 03	3600	10 – 15
J1335+0824	13:35:32.7	+08:24:04.3	1.91	19.0	C1	2x2	2012 April 15	3000	5 – 8
J1417+4132	14:17:19.2	+41:32:37.0	2.02	18.4	C5	2x2	2006 June 03	25200	13 – 52
J1454+0941	14:54:35.2	+09:41:00.1	1.95	18.6	C1	2x2	2012 April 15	2400	13 – 17
J1509+1113	15:09:32.1	+11:13:13.7	2.11	19.0	C1	2x2	2012 April 15	5194	5 – 12
J1524+1030	15:24:30.05	+10:30:32.0	2.06	18.2	C1	2x1	2011 July 04	9000	4 – 11
J1552+4910	15:52:33.9	+49:10:08.3	2.04	18.0	C1	2x1	2005 May 03	9000	15 – 25
J1555+4800	15:55:56.9	+48:00:15.1	3.30	19.1	C5	2x1	2006 June 04	21600	10 – 16
J1610+4724	16:10:09.4	+47:24:44.5	3.22	18.6	C1	2x1	2006 August 18	24900	5 – 12
J1629+0913	16:29:03.0	+09:13:22.5	1.99	18.2	C1	2x2	2012 April 15	2400	9 – 14
Q1755+578	17:56:03.6	+57:48:48.0	2.11	18.6	C1	2x1	2006 August 20	41200	4 – 16
J2241+1225	22:41:45.1	+12:25:57.1	2.63	17.9	C1	2x1	2007 September 17	7200	5 – 7

the average S/N of the 200 Å centered around the Lyman- α line³, and the derived HI column density (see Section 3.1) of the absorber are shown in Table 2. The data were reduced using the publicly available **Low-Redux** pipeline developed by J. Hennawi, S. Burles, D. Schlegel, and J. X. Prochaska⁴.

3. The Data

3.1. HI Column densities

We determine the HI column density, $N(\text{HI})$, of an absorber in a quasar spectrum by simultaneously fitting the continuum of the background quasar and fitting a Voigt profile to the Ly- α line of the absorber. This method yields an accurate HI column density, if the continuum of the quasar can be accurately placed. For cases where we did not obtain follow-up observations with a blue-sensitive spectrograph, we adopt the following procedure to measure the HI column density directly from the HIRES spectra. First, we observe a spectroscopic standard star of known flux at the same instrument settings as the absorber. Dividing the observed spectra of the star by the known flux yields a response function for each order. This response function is then used to find the relative flux of the absorber spectrum. Suzuki et al. (2003) noted that because of the peculiarities of the HIRES instrument, they found that the fluxed spectra can be off by as much as 10%. To account for this systematic error, we apply a 10% adjustment to the spectra and then refit the absorber. Any differences in column densities between the measurements are then included in the uncertainty of the HI column density. Figure 1 shows the fit of the Ly- α line for the 18 absorbers below $z \sim 2.2$ without follow-up observations using the BCS. Note that the flux has been normalized and binned into bins of $\sim 20 \text{ km s}^{-1}$ for visual presentation.

To test the accuracy of using HIRES to determine $N(\text{HI})$, we have followed up 4 absorbers with the blue-sensitive Kast spectrograph on the Shane-3m telescope (Figure 1). The normalized

³Around the Ly- α line, Ly α forest absorption (which may not be resolved in low resolution observations) contaminates the spectra which reduces the S/N. The S/N measurements should be taken as a lower limit, where values of S/N > 4 are acceptable.

⁴<http://www.ucolick.org/~xavier/LowRedux/>

Table 2: Kast Journal of Observations

QSO	RA (J2000.0)	DEC (J2000.0)	z_{em}	Date Observed	Exposure Time (s)	S/N pixel ⁻¹	logN(HI)
J0233+0103	02 33 33.2	+01 03 33.0	2.060	2011 Aug 28	3600	5	20.45 ± 0.15
J0958+0145	09 58 22.2	+01 45 24.2	1.960	2012 Feb 21	3600	4	20.30 ± 0.15
J1313+1441	13 13 41.2	+14 41 40.6	1.884	2012 Feb 20	3600	9	21.20 ± 0.15
J1629+0913	16 29 02.9	+09 13 22.5	1.986	2011 Aug 28	3600	5	20.80 ± 0.15

spectra are shown in blue for these 4 absorbers. The resulting HI column densities measured from these spectra (listed in Table 2) are within 0.1 dex from those measured using the HIRES spectra, well within the uncertainty of each measurement. As a result we are confident that the N(HI) measurements for the remaining DLAs only observed with HIRES are accurate, and thus adopt the HIRES-derived HI column densities for these 18 DLAs. The complete list of HI measurements are tabulated in Table 3.

3.2. Metal Column Densities

As in previous, large surveys of metal column densities (e.g. Prochaska et al. 2001b), all metal column densities measured for the cMSDLA sample (given in Table 4) were obtained using the apparent optical depth method (AODM) outlined by Savage & Sembach (1991). The AODM provides accurate column densities for non-saturated and non-blended lines, and is faster than fitting Voigt profiles for each individual system. The AODM sums the optical depth (τ) of an unsaturated absorption line (at wavelength λ , with oscillator strength f) and is converted to a column density (N) using

$$N = \frac{m_e c}{\pi e^2 f \lambda} \int \tau dv \quad (1)$$

where the integral of the optical depth sums over each pixel in velocity space. The limits for the optical depth integration are chosen to contain the absorption profile that is common to all non-contaminated transitions. For lines that were either blended or saturated (and no other *clean* transitions were available for the same species), the derived AODM column density was taken as an upper or lower limit (respectively). The errors quoted on the column densities (N_{err}) were determined from the error spectrum using

$$N_{err} = \frac{m_e c}{\pi e^2 f \lambda} \left(\sum \left(\frac{I_{err}}{I_{spec}} \Delta v \right)^2 \right)^{0.5} \quad (2)$$

where I_{err} and I_{spec} are the fluxes in the error and observed spectra (respectively), and Δv is the velocity width of the pixel. The error spectrum only accounts for photon noise, and not continuum errors. A minimum error of 0.05 dex is adopted for all metal columns to account for any systematic errors (such as continuum placement).

For each DLA sight-line, all transitions seen for the elements Fe, Zn, S, Si, Cr, Mn, and Ni are shown in Figures 2–32⁵, with the AODM velocity limits and column densities given in Tables A.1–A.31. The adopted column densities in Tables A.1–A.31 (N_{adopt}) are determined from the

⁵Figures 3–32 are provided in the published version of this paper in PASP (online edition only). Figure 2 is provided as an example.

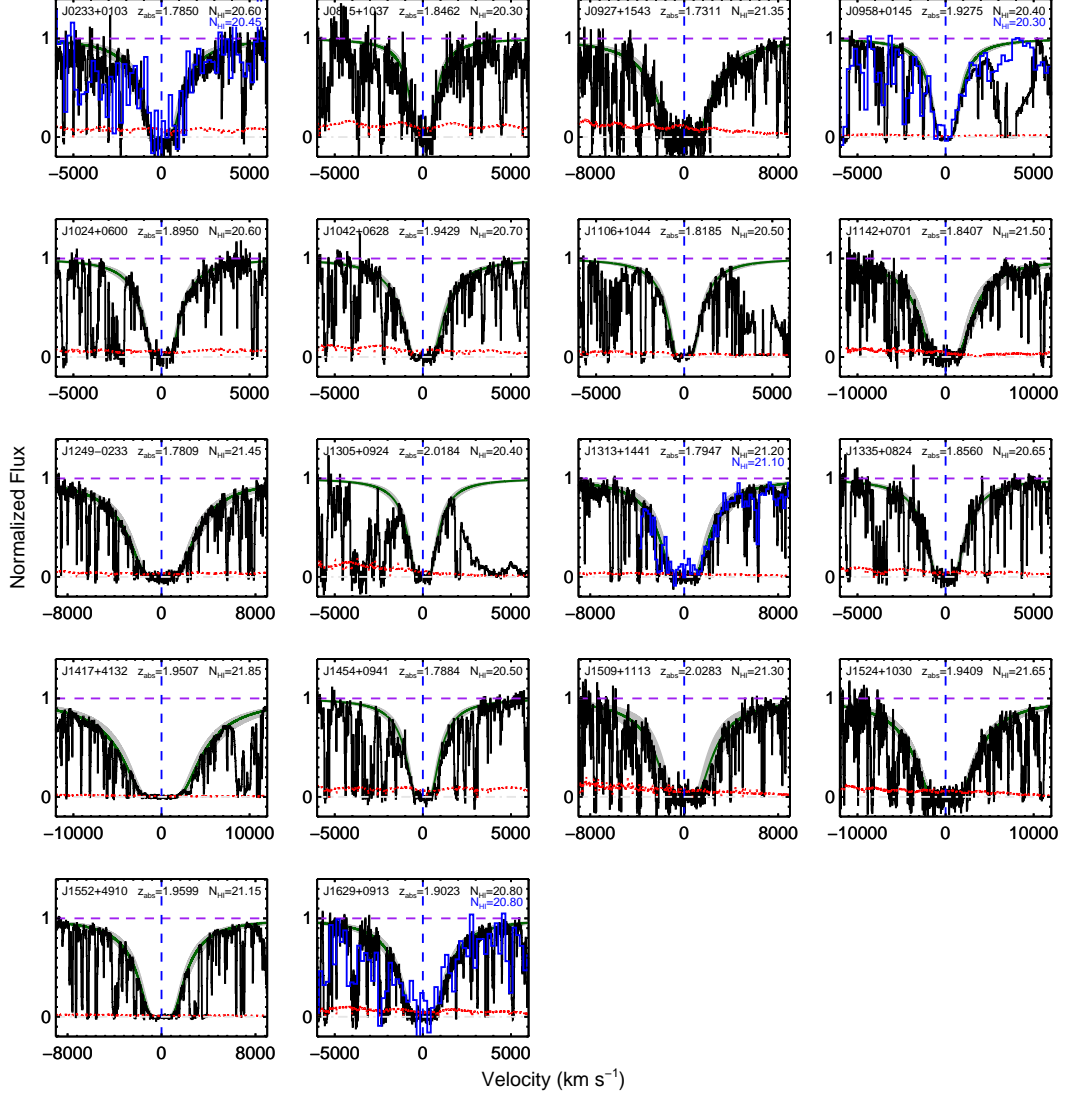


Fig. 1.— Voigt profile fits of the Ly- α transition of the 18 absorbers below $z \sim 2.2$ not observed with the BCS on MMT (Kaplan et al. 2010). The gray shaded area marks the 95 % confidence limits to the fit. The dotted (red) line is the 1- σ error on the observation, the vertical dashed (blue) line marks the absorber’s redshift measured from the metal lines, and the horizontal dashed (purple) line marks the normalized continuum of the spectrum. For the 4 DLAs observed with the Kast spectrograph, the Kast spectrum is overplotted in blue. The HI column densities for these 4 DLAs observed with Kast are provided in blue below the HIRES-derived $N(\text{HI})$.

Table 3: HI column densities of MSDLA candidates

QSO	z_{em}	z_{abs}	$\log N(\text{HI})$	Reference
J0008–0958	1.95	1.7675	20.85 ± 0.15	1, 2
J0044+0018	1.87	1.7250	20.35 ± 0.10	2, 3
J0058+0115	2.50	2.0095	21.10 ± 0.10	1, 4
J0211+1241	2.95	2.5951	20.60 ± 0.15	2
J0233+0103	2.06	1.7850	20.60 ± 0.15	2
J0815+1037	2.02	1.8462	20.30 ± 0.15	2
J0927+1543	1.80	1.7311	21.35 ± 0.15	2
J0927+5823	1.91	1.6352	20.40 ± 0.15	3
J0958+0145	1.96	1.9275	20.40 ± 0.10	2
J1013+5615	3.61	2.2831	20.70 ± 0.15	2
J1024+0600	2.13	1.8950	20.60 ± 0.15	2
J1042+0628	2.04	1.9429	20.70 ± 0.15	2
J1049–0110	2.12	1.6577	21.35 ± 0.15	1, 3
J1056+1208	1.92	1.6093	21.45 ± 0.15	2, 3, 5
J1106+1044	1.86	1.8185	20.50 ± 0.15	2
J1142+0701	1.87	1.8407	21.50 ± 0.15	2
J1155+0530	3.48	3.3260	21.05 ± 0.10	6
J1305+0924	2.06	2.0184	20.40 ± 0.15	2
J1310+5424	1.93	1.8006	21.45 ± 0.15	2, 3, 5
J1313+1441	1.88	1.7947	21.20 ± 0.15	2
J1335+0824	1.91	1.8560	20.65 ± 0.15	2
J1417+4132	2.02	1.9509	21.85 ± 0.15	2, 4
J1454+0941	1.95	1.7884	20.50 ± 0.15	2
J1509+1113	2.11	2.0283	21.30 ± 0.15	2
J1524+1030	2.06	1.9409	21.65 ± 0.15	2
J1552+4910	2.04	1.9599	21.15 ± 0.15	2
J1555+4800	3.30	2.3911	21.50 ± 0.15	2
J1610+4724	3.22	2.5066	21.00 ± 0.15	3
J1629+0913	1.99	1.9023	20.80 ± 0.10	2
Q1755+578	2.11	1.9692	21.40 ± 0.15	2
J2241+1225	2.63	2.4179	21.15 ± 0.10	2

REFERENCES– (1) Herbert-Fort et al. (2006). (2) This Work. (3) Kaplan et al. (2010). (4) Berg et al. (2013). (5) Prochaska et al. (2008). (6) Wolfe et al. (2008).

included lines using a weighted mean⁶. In cases where we suspect *mild* saturation, we fit a Voigt profile using VPFIT⁷ to test whether the AODM column densities are accurate. We discuss any subtleties of the measurements on a case by case basis below. For all plots of the metal line profiles, the horizontal dashed line shows the continuum, while the vertical dotted lines show the velocity limits for the AODM integration to obtain the column density. All bad pixels within each plot are grayed out. All atomic data were taken from Morton (2003).

3.2.1. J0008–0958

The SiII λ 1253 absorption is strongly blended with the Ly α forest, and is ignored from the adopted SiII column density. We adopt the Zn column density obtained solely from the ZnII λ 2026 line. There appears to be some slight blending at $\sim -160\text{km s}^{-1}$ at the ZnII λ 2062 line, likely from CrII λ 2062 contamination, causing an overestimate of the obtained column density for the redder transition.

3.2.2. J0044+0018

The DLA towards J0044+0018 is believed to have a large amount of cold gas, as indicated by the detection of Cl. As a result, the DLA likely has a large amount of MgI present, contaminating the ZnII λ 2026 line (e.g. HF06 and references therein). It is clear in Figure 3 that the ZnII λ 2026 line has a slight double peak for each absorption component relative to the other lines, due to blending from MgI. We therefore treat the measured $N(\text{ZnII})$ as an upper limit.

3.2.3. J0058+0115

For the DLA towards J0058+0115, we quote a detection of the ZnII column density, despite having a dead pixel within the absorption at $\sim 0\text{km s}^{-1}$. The dead pixel only contributes ~ 0.02 dex to the total column density (within the quoted error), and is therefore adopted without any corrections.

⁶Each line is weighted by N_{err}^{-2} (solely derived from the error spectrum) in order to reflect the quality of the spectra at each line.

⁷<http://www.ast.cam.ac.uk/~rfc/vpfit.html>

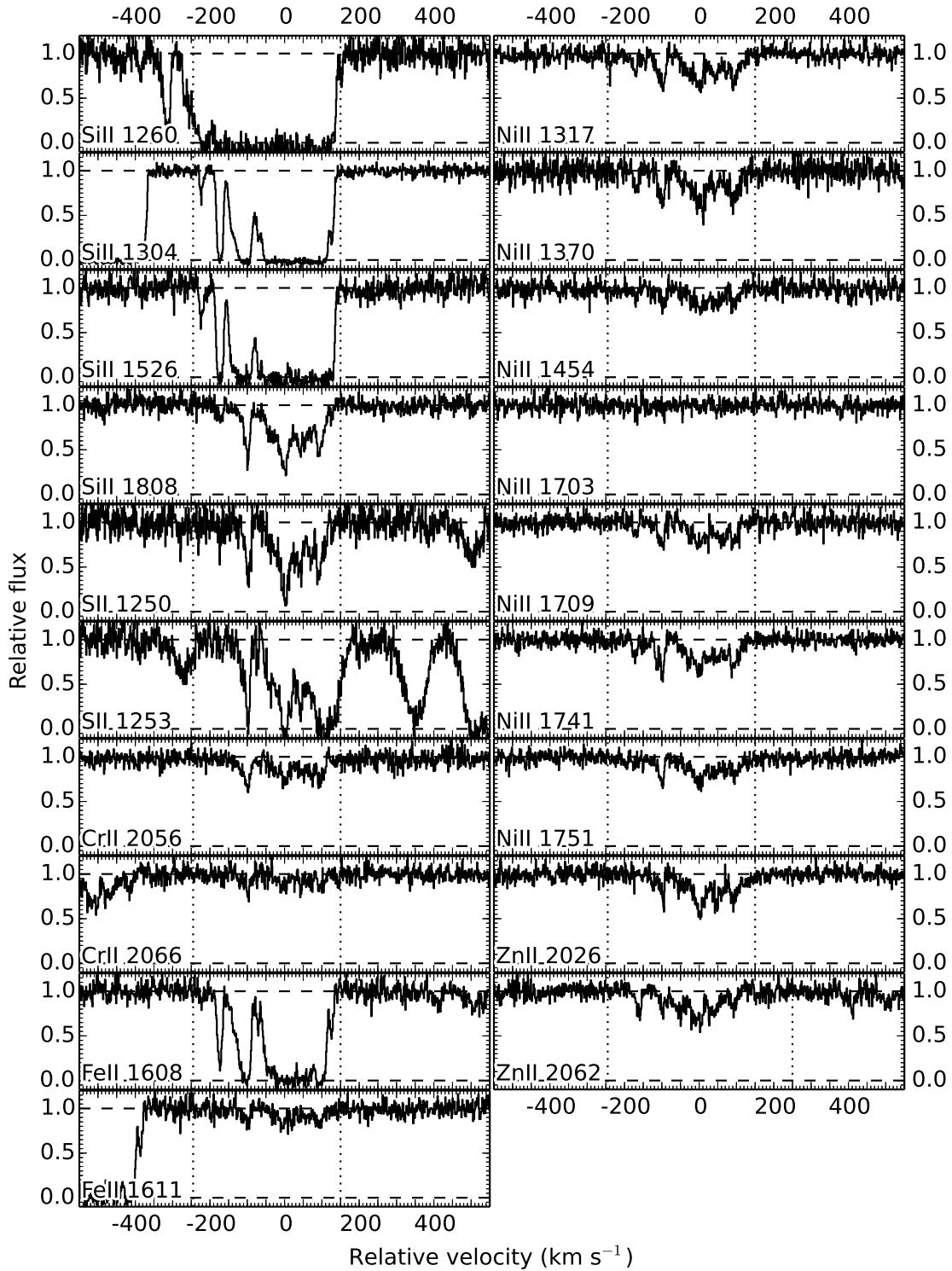


Fig. 2.— Metal line velocity profiles for J0008–0958.

3.2.4. *J0211+1241*

Although the SiII λ 1253 line is covered in our spectrum, there is severe contamination with a Ly α forest cloud, so no measurement is provided.

3.2.5. *J0233+0103*

Although both SiII λ 1304 and 1526 lines appear saturated, we can constrain N(SiII) in the DLA towards J0233+0103 using the upper limit of the column density derived using SiII λ 1808 line. With both upper and lower limits obtained from these three lines, the total SiII column density should be $N(\text{SiII}) \sim 14.77 \pm 0.05$.

3.2.6. *J0815+1037*

We note that the error on the column density derived for Si II λ 1808 in the DLA towards J0815+1037 is very high (0.45 dex) compared to the typical error in metal column densities. The adopted error reflects the low S/N in the spectrum ($S/N \sim 2-3$) for the weak line.

3.2.7. *J0927+1543*

For the DLA detected towards J0927+1543 sight-line, both FeII λ 1608 and 1611 lines provide tight constraints on the true N(FeII) of the system, and are averaged together to obtain the final adopted column density.

3.2.8. *J0958+0145*

Although there is clearly some absorption of ZnII λ 2026 in the spectrum of J0958+0145 with the same expected absorption profile for a line of this strength (see Figure 10), we quote N(ZnII) as an upper limit. As the strongest component of the ZnII λ 2026 absorption is offset from by $\sim 10\text{km s}^{-1}$ relative to other metal lines, we are cautious to deem our measured column density as a detection. We therefore conservatively quote the adopted column density as an upper limit.

3.2.9. *J1013+5615*

In the DLA towards J1013+5615, both CrII λ 2056 and ZnII λ 2026 contain bad pixels within the absorption features. Although the determined column density was derived including these bad

pixels; the bad pixels have a negligible effect on the total column density (0.002 and 0.021 dex, respectively). The final column densities are not adjusted as a result of the bad pixels.

3.2.10. *J1042+0628*

The lower and upper limits in the derived column densities for FeII λ 1608 and 1611 (respectively) provide constraining bounds on the expected $N(\text{FeII})$ in J1042+0628. As a result, we assume an average of the two limits ($N(\text{FeII})=15.00 \pm 0.15$) as the adopted column density for this DLA.

3.2.11. *J1056+1208*

Even though the SiII λ 1808 line is slightly saturated, we can get a robust measurement by using a chi-squared fitting routine, VPFIT. We tied the velocity structure of the SiII line to the unsaturated ZnII line and measured the column density. We compared the VPFIT-derived column density to the AODM-derived column density and found the two to be in agreement within the error of the measurements.

3.2.12. *J1142+0701*

Si II λ 1808 appears saturated in the spectrum of the DLA towards J1142+0701. To verify the effects of saturation, VPFIT was used to determine the column density (similar to the procedure describe for the DLA in J1056+1208). The VPFIT column density agrees with the AODM derived column density given.

3.2.13. *J1305+0924*

For the DLA in the J1305+0924 spectrum, the absorption feature from SII λ 1259 is slightly blended with a Ly α cloud in the highest velocity component (75 km s^{-1}). With the lack of absorption beyond 75 km s^{-1} seen in the other metal lines, truncating the AODM limit for SII λ 1259 at 75 km s^{-1} should have a negligible effect on the total column density derived, and is still consistent with the other SII lines.

3.2.14. *J1313+1441*

For this DLA, we are only able to obtain lower limits on $N(\text{SII})$ from the SII λ 1250 and 1253 lines due to saturation. Although SII λ 1253 provides the more constraining limit, there appears to

be unrelated absorption at $\sim 100\text{km s}^{-1}$. As a result, we ignore this more constraining limit. In Berg et al. (2013), we had originally reported the sulphur column density as a detection rather than a limit, as it is unclear whether the SII λ 1250 line is saturated. To be conservative, we have decided to adopt the derived column density as a lower limit. Similar to the DLA towards J1056+1208; we have used VPFIT to check the derived column density from SiII λ 1808 and find agreement with the AODM derived column density.

3.2.15. J1417+4132

Although a limit of $\log N(\text{S}) > 15.8$ was initially reported from the data in Berg et al. (2013) as it appears saturated, the SII data is too blended to place a constraining limit on the derived column density. To be consistent with other DLAs we have previously discussed, we do not include such a limit as we are unsure of the role of saturation and contamination to place a meaningful limit on the column density.

3.2.16. J1555+4800

The J1555+4800 spectrum shows a Ly α cloud blended with SII λ 1253, making it impossible to determine the amount of saturation and blending to provide a meaningful limit. However, it is worth noting that assuming that the absorption is real, a lower limit of $\log N(\text{S}) > 15.88$ was measured for this system (Berg et al. 2013).

3.2.17. Q1755+578

The DLA towards Q1755+578 is a system with a large amount of CI (i.e. a significant amount of cold gas). It is clear in Figure 31 for ZnII λ 2056 there is an additional narrow absorption at $\sim 50\text{km s}^{-1}$, that is likely due to MgI absorption. From Voigt profile modelling of this complex system, we obtained a column density of $N(\text{ZnII}) = 13.85 \pm 0.05$.

3.2.18. J2241+1225

The SII column density for J2241+1225 challenging due to uncertain levels of saturation of the SII λ 1253 and 1259. As SII λ 1259 appears to have a slight excess of absorption at $\sim -60\text{km s}^{-1}$ relative to the typical absorption profile for this system, we adopt the value from SII λ 1253. Although it is likely that the line is not saturated (as originally claimed in Berg et al. 2013, $N(\text{SII}) = 14.94 \pm 0.05$), we remain conservative and keep this value as a lower limit.

Table 4: Summary of Column Densities

QSO	z_{em}	z_{abs}	$\log N(\text{H I})$	$\log N(\text{Si II})$	$\log N(\text{S II})$	$\log N(\text{Mn II})$	$\log N(\text{Cr II})$	$\log N(\text{Fe II})$	$\log N(\text{Ni II})$	$\log N(\text{Zn II})$
J0008-0958	1.95	1.7675	20.85 ± 0.15	16.04 ± 0.05	15.84 ± 0.05	...	13.91 ± 0.05	15.62 ± 0.05	14.46 ± 0.05	13.31 ± 0.05
J0044+0018	1.87	1.7250	20.35 ± 0.10	15.34 ± 0.05	15.27 ± 0.05	...	< 13.04	> 14.77	13.89 ± 0.05	< 12.61
J0058+0115	2.50	2.0095	21.10 ± 0.10	> 15.55	15.40 ± 0.05	...	13.54 ± 0.05	15.18 ± 0.05	14.16 ± 0.05	12.95 ± 0.05
Q0201+36	2.91	2.4628	20.38 ± 0.04	15.53 ± 0.05	15.29 ± 0.05	...	13.24 ± 0.05	15.01 ± 0.05	14.03 ± 0.05	12.76 ± 0.05
J0211+1241	2.95	2.5951	20.60 ± 0.15	15.53 ± 0.08	15.06 ± 0.05	14.07 ± 0.05	...
J0233+0103	2.06	1.7850	20.60 ± 0.15	14.77 ± 0.05	14.62 ± 0.05	13.61 ± 0.11	...
Q0458-02	2.29	2.0396	21.65 ± 0.09	16.04 ± 0.05	13.76 ± 0.05	15.38 ± 0.05	14.18 ± 0.05	13.13 ± 0.05
FJ0812+3208	2.70	2.6263	21.35 ± 0.10	15.98 ± 0.05	15.63 ± 0.07	< 13.00	13.36 ± 0.05	15.09 ± 0.05	13.89 ± 0.05	13.15 ± 0.05
J0815+1037	2.02	1.8462	20.30 ± 0.15	15.38 ± 0.45	> 14.87	13.74 ± 0.12	...
J0927+1543	1.80	1.7311	21.35 ± 0.15	15.99 ± 0.05	13.83 ± 0.05	15.14 ± 0.24	14.17 ± 0.05	13.38 ± 0.05
J0927+5823	1.91	1.6352	20.40 ± 0.15	15.72 ± 0.05	15.61 ± 0.05	> 15.27	14.44 ± 0.05	13.29 ± 0.05
J0958+0145	1.96	1.9275	20.40 ± 0.10	14.84 ± 0.06	14.44 ± 0.05	14.23 ± 0.05	13.37 ± 0.07	< 12.00
J1010+0003	1.40	1.2651	21.52 ± 0.07	13.54 ± 0.07	15.26 ± 0.05	...	12.96 ± 0.06
J1013+5615	3.61	2.2831	20.70 ± 0.15	16.14 ± 0.05	13.79 ± 0.05	> 15.45	...	13.56 ± 0.05
J1024+0600	2.13	1.8950	20.60 ± 0.15	15.81 ± 0.05	15.45 ± 0.05	15.27 ± 0.08	14.02 ± 0.05	...
J1042+0628	2.04	1.9429	20.70 ± 0.15	15.40 ± 0.08	15.08 ± 0.05	15.00 ± 0.15	< 13.78	...
J1049-0110	2.12	1.6577	21.35 ± 0.15	15.80 ± 0.05	15.47 ± 0.05	...	13.49 ± 0.05	15.17 ± 0.05	14.25 ± 0.05	13.14 ± 0.05
J1056+1208	1.92	1.6093	21.45 ± 0.15	16.48 ± 0.09	> 16.15	...	14.04 ± 0.05	15.81 ± 0.05	14.69 ± 0.05	13.76 ± 0.05
J1106+1044	1.86	1.8185	20.50 ± 0.15	> 15.22	15.33 ± 0.05	> 15.15	14.02 ± 0.05	...
J1142+0701	1.87	1.8407	21.50 ± 0.15	16.15 ± 0.13	13.70 ± 0.05	15.47 ± 0.05	14.01 ± 0.05	13.29 ± 0.05
J1155+0530	3.48	3.3260	21.05 ± 0.10	15.94 ± 0.05	15.40 ± 0.05	...	13.36 ± 0.09	15.37 ± 0.05	14.07 ± 0.05	12.89 ± 0.07
J1159+0112	1.99	1.9440	21.70 ± 0.10	15.95 ± 0.05	...	< 13.26	13.82 ± 0.05	15.49 ± 0.05	14.20 ± 0.05	13.11 ± 0.06
J1200+4015	3.36	3.2200	20.85 ± 0.10	> 15.21	15.36 ± 0.05	...	13.53 ± 0.05	15.31 ± 0.05	14.18 ± 0.05	12.86 ± 0.05
J1249-0233	2.12	1.7809	21.45 ± 0.15	> 15.11	15.53 ± 0.05	14.29 ± 0.05	13.15 ± 0.05
J1305+0924	2.06	2.0184	20.40 ± 0.15	15.75 ± 0.05	15.39 ± 0.05	15.21 ± 0.14	14.36 ± 0.05	...
J1310+5424	1.93	1.8006	21.45 ± 0.15	16.44 ± 0.05	> 16.05	...	13.99 ± 0.05	15.64 ± 0.05	14.45 ± 0.05	13.57 ± 0.05
J1313+1441	1.88	1.7947	21.20 ± 0.15	16.12 ± 0.05	> 15.75	...	13.61 ± 0.05	15.55 ± 0.05	14.27 ± 0.05	13.30 ± 0.05
J1335+0824	1.91	1.8560	20.65 ± 0.15	15.73 ± 0.05	15.29 ± 0.05	13.70 ± 0.10	13.81 ± 0.05	> 15.17	14.29 ± 0.05	...
J1417+4132	2.02	1.9509	21.85 ± 0.15	> 16.42	14.04 ± 0.05	15.58 ± 0.05	14.55 ± 0.05	13.55 ± 0.05
J1454+0941	1.95	1.7884	20.50 ± 0.15	15.47 ± 0.05	15.25 ± 0.06	...	13.30 ± 0.09	15.02 ± 0.12	13.85 ± 0.05	12.72 ± 0.05
J1509+1113	2.11	2.0283	21.30 ± 0.15	16.04 ± 0.05	15.69 ± 0.05	15.48 ± 0.07	14.41 ± 0.05	...
J1524+1030	2.06	1.9409	21.65 ± 0.15	> 16.24	> 15.63	...	13.57 ± 0.05	15.44 ± 0.05	14.53 ± 0.05	> 13.53
J1552+4910	2.04	1.9599	21.15 ± 0.15	15.98 ± 0.05	15.34 ± 0.05	13.39 ± 0.05	13.74 ± 0.05	15.47 ± 0.05	14.24 ± 0.05	12.93 ± 0.05
J1555+4800	3.30	2.3911	21.50 ± 0.15	16.55 ± 0.05	14.19 ± 0.05	15.84 ± 0.05	14.78 ± 0.05	< 13.95
J1604+3951	3.15	3.1633	21.75 ± 0.00	> 15.31	15.71 ± 0.05	15.47 ± 0.05	14.24 ± 0.05	13.12 ± 0.05
J1610+4724	3.22	2.5066	21.00 ± 0.15	16.16 ± 0.05	13.90 ± 0.05	15.62 ± 0.05	14.58 ± 0.05	13.56 ± 0.05
J1629+0913	1.99	1.9023	20.80 ± 0.10	15.32 ± 0.06	15.24 ± 0.05	...	< 13.21	> 14.93	13.75 ± 0.13	12.68 ± 0.08
Q1755+578	2.11	1.9692	21.40 ± 0.15	16.58 ± 0.05	> 16.12	13.83 ± 0.05	14.09 ± 0.05	15.79 ± 0.05	14.75 ± 0.05	13.85 ± 0.05
J2100-0641	3.14	3.0924	21.05 ± 0.15	15.88 ± 0.05	15.49 ± 0.05	...	13.59 ± 0.05	15.37 ± 0.05	14.23 ± 0.05	13.24 ± 0.05
J2222-0946	2.93	2.3543	20.55 ± 0.15	15.68 ± 0.05	15.37 ± 0.05	15.06 ± 0.08	14.04 ± 0.05	...
Q2230+02	2.15	1.8644	20.85 ± 0.08	15.65 ± 0.05	15.29 ± 0.05	...	13.40 ± 0.05	15.19 ± 0.05	14.13 ± 0.05	12.80 ± 0.05
J2241+1225	2.63	2.4179	21.15 ± 0.10	> 14.67	> 15.01	13.36 ± 0.13	...	15.02 ± 0.08	13.83 ± 0.05	...
J2340-0053	2.09	2.0545	20.35 ± 0.15	15.23 ± 0.05	14.95 ± 0.05	14.98 ± 0.05	13.81 ± 0.05	12.63 ± 0.07
Q2342+34	2.92	2.9082	21.10 ± 0.10	15.62 ± 0.05	15.19 ± 0.05	...	13.23 ± 0.11	14.91 ± 0.07	13.81 ± 0.05	< 12.60

4. Summary

4.1. Sample Properties

A summary of all the properties of the entire cMSDLA sample (literature and new observations) is provided in Table 5. Included in Table 5 are the metallicities (following the scheme in Rafelski et al. 2012, R12), whether or not the DLA is a bona fide MSDLA, and the velocity width of the inner 90% of the metal lines (Δv_{90} ; see Prochaska & Wolfe 1997). It is interesting to note that the majority of DLAs in our sample have $\Delta v_{90} \gtrsim 100 \text{ km s}^{-1}$, implying that these systems live in some of the most massive dark matter halos in which DLAs reside (see Neeleman et al. 2013).

Figures 33, 34, and 35 show the distributions of neutral hydrogen column density, metallicity (using the solar scale from Asplund et al. 2009), and absorption redshift of our cMSDLA sample in comparison to a sample of DLAs from the literature compiled by R12. The R12 sample is a compilation of metal abundances of DLAs published in the literature from studies that do not specifically target metal-poor or metal-strong systems. We have removed all the DLAs from the R12 sample that also appear in our cMSDLA sample. However, it is important to note that there are MSDLAs still present within the R12 sample after removing the duplicated DLAs from our sample ($\sim 6\%$; see discussion below).

Figure 33 clearly shows that the distribution of neutral hydrogen column density for the cMSDLA sample spans the entire range of values as the DLAs in the R12 sample. However the cMSDLA sample shows a bias to higher $N(\text{HI})$ systems in contrast to what is seen in the R12 sample (and other $N(\text{HI})$ distributions seen for larger surveys, see Noterdaeme et al. 2012, for example). It is likely that due to selecting larger metal column densities, high metal column density DLAs tend to probe more gas-rich systems and thus have higher HI column densities relative to a typical DLA (Kaplan et al. 2010). This excess of high $N(\text{HI})$ DLAs is seen in Figure 33, where nearly half of the cMSDLAs in our sample have hydrogen column densities of $\log N(\text{HI}) \sim 21$, whereas the median HI column density for the R12 literature sample is $N(\text{HI}) = 20.7$. Furthermore, a KS test rules out that the two populations are drawn from the same parent sample at a 98.6% confidence level.

The metallicity distributions of the cMSDLA and R12 samples are shown in Figure 34. Whereas the median metallicity of the R12 literature DLAs is $[\text{M}/\text{H}] = -1.51$, this value is the lowest metallicity of the cMSDLA sample distribution. We can safely say that the cMSDLA sample is indeed *metal-rich* relative to the average DLA in the literature. Furthermore, the use of sulphur as a metallicity indicator is preferentially selected in the cMSDLA sample, as the higher column densities allow for more frequent detections of the weaker SII lines. For comparison, the typical metallicity indicator in the R12 DLAs is SiII.

In terms of redshift (Figure 35), the cMSDLA sample does not span the entire range that the R12 literature DLA sample spans, but fall mostly within the redshift range of 1.5 to 3.5. This range in redshift is entirely due to selection effects; from choosing DLAs where the $[\text{CII}] \lambda 158$ micron emission with ALMA, and observing both Ly- α and metal lines from ground-based

Table 5: Summary of cMSDLA Sample

QSO	z_{abs}	$\log N(\text{H I})$	[M/H] (elem)	MSDLA?	Δv_{90} (line) km s ⁻¹	Ref.
J0008–0958	1.7675	20.85 ± 0.15	–0.16 ± 0.16 (S)	True	216 (SiII 1808)	1,2
J0044+0018	1.7250	20.35 ± 0.10	–0.23 ± 0.11 (S)	False	172 (SiII 1253)	2
J0058+0115	2.0095	21.10 ± 0.10	–0.85 ± 0.11 (S)	False	195 (SiII 1253)	1,2
Q0201+36	2.4628	20.38 ± 0.04	–0.24 ± 0.07 (S)	False	200 (SiII 1808)	1,3,4,5,6
J0211+1241	2.5951	20.60 ± 0.15	–0.58 ± 0.17 (Si)	False	48 (NiII 1741)	2
J0233+0103	1.7850	20.60 ± 0.15	–1.34 ± 0.16 (Si)	False	97 (FeII 1608)	2
Q0458–02	2.0396	21.65 ± 0.09	–1.12 ± 0.10 (Si)	True	84 (CrII 2056)	1,2,5,7,8
FJ0812+3208	2.6263	21.35 ± 0.10	–0.87 ± 0.12 (S)	True	56 (SiII 1250)	1,2,9,10
J0815+1037	1.8462	20.30 ± 0.15	–0.43 ± 0.47 (Si)	False	–99 (no line)	2
J0927+1543	1.7311	21.35 ± 0.15	–0.87 ± 0.16 (Si)	True	220 (SiII 1808)	1,2
J0927+5823	1.6352	20.40 ± 0.15	0.06 ± 0.16 (S)	True	208 (SiII 1808)	1,2
J0958+0145	1.9275	20.40 ± 0.10	–1.11 ± 0.11 (S)	False	56 (SiII 1259)	1,2
J1010+0003	1.2651	21.52 ± 0.07	–1.19 ± 0.10 (Zn)	False	36 (NiII 1709)	1,2,11,12
J1013+5615	2.2831	20.70 ± 0.15	–0.07 ± 0.16 (Si)	True	213 (SiII 1808)	1,2
J1024+0600	1.8950	20.60 ± 0.15	–0.30 ± 0.16 (S)	False	161 (SiII 1808)	2
J1042+0628	1.9429	20.70 ± 0.15	–0.77 ± 0.16 (S)	False	135 (SiII 1253)	2
J1049–0110	1.6577	21.35 ± 0.15	–1.03 ± 0.16 (S)	False	330 (SiII 1808)	1,2
J1056+1208	1.6093	21.45 ± 0.15	–0.48 ± 0.18 (Si)	True	124 (NiII 1370)	1,2
J1106+1044	1.8185	20.50 ± 0.15	–0.32 ± 0.16 (S)	False	203 (SiII 1253)	2
J1142+0701	1.8407	21.50 ± 0.15	–0.86 ± 0.20 (Si)	True	52 (NiII 1370)	2
J1155+0530	3.3260	21.05 ± 0.10	–0.80 ± 0.11 (S)	False	220 (SiII 1250)	1,2
J1159+0112	1.9440	21.70 ± 0.10	–1.26 ± 0.11 (Si)	True	84 (NiII 1741)	1,2,13,14,15
J1200+4015	3.2200	20.85 ± 0.10	–0.64 ± 0.11 (S)	False	127 (NiII 1317)	1,2,16
J1249–0233	1.7809	21.45 ± 0.15	–1.07 ± 0.16 (S)	True	152 (SiII 1250)	1,2,17
J1305+0924	2.0184	20.40 ± 0.15	–0.16 ± 0.16 (S)	False	135 (SiII 1253)	2
J1310+5424	1.8006	21.45 ± 0.15	–0.52 ± 0.16 (Si)	True	86 (NiII 1751)	1,2
J1313+1441	1.7947	21.20 ± 0.15	–0.59 ± 0.16 (Si)	True	147 (ZnII 2026)	1,2
J1335+0824	1.8560	20.65 ± 0.15	–0.51 ± 0.16 (S)	False	166 (SiII 1253)	2
J1417+4132	1.9509	21.85 ± 0.15	–0.93 ± 0.16 (Zn)	True	114 (ZnII 2026)	1,2
J1454+0941	1.7884	20.50 ± 0.15	–0.40 ± 0.16 (S)	False	81 (SiII 1253)	2
J1509+1113	2.0283	21.30 ± 0.15	–0.76 ± 0.16 (S)	True	101 (SiII 1253)	2
J1524+1030	1.9409	21.65 ± 0.15	–1.36 ± 0.16 (Fe)	True	201 (NiII 1709)	1,2
J1552+4910	1.9599	21.15 ± 0.15	–0.96 ± 0.16 (S)	True	112 (SiII 1808)	1,2
J1555+4800	2.3911	21.50 ± 0.15	–0.46 ± 0.16 (Si)	True	199 (NiII 1741)	1,2
J1604+3951	3.1633	21.75 ± 0.00	–1.19 ± 0.05 (S)	False	429 (SiII 1250)	1,2,18
J1610+4724	2.5066	21.00 ± 0.15	–0.35 ± 0.16 (Si)	True	155 (SiII 1808)	1,2,17
J1629+0913	1.9023	20.80 ± 0.10	–0.71 ± 0.11 (S)	False	117 (SiII 1253)	2
Q1755+578	1.9692	21.40 ± 0.15	–0.33 ± 0.16 (Si)	True	364 (NiII 1741)	1,2
J2100–0641	3.0924	21.05 ± 0.15	–0.71 ± 0.16 (S)	True	187 (SiII 1250)	1,2,17
J2222–0946	2.3543	20.55 ± 0.15	–0.33 ± 0.16 (S)	False	173 (SiII 1253)	1,2,17,19
Q2230+02	1.8644	20.85 ± 0.08	–0.71 ± 0.10 (S)	False	172 (SiII 1808)	1,2,5,7,8,14,15
J2241+1225	2.4179	21.15 ± 0.10	–1.28 ± 0.13 (Fe)	False	65 (SiII 1253)	1,2
J2340–0053	2.0545	20.35 ± 0.15	–0.55 ± 0.16 (S)	False	138 (SiII 1808)	1,2,10
Q2342+34	2.9082	21.10 ± 0.10	–1.06 ± 0.11 (S)	False	100 (SiII 1808)	1,2,9,10

REFERENCES– (1) Berg et al. (2013). (2) This Work. (3) Prochaska & Wolfe (1996). (4) Pettini et al. (1997). (5) Prochaska et al. (2001c). (6) Prochaska et al. (2002). (7) Prochaska & Wolfe (1999). (8) Prochaska et al. (2001a). (9) Prochaska et al. (2003b). (10) Prochaska et al. (2007). (11) Meiring et al. (2006). (12) Nestor et al. (2008). (13) Petitjean et al. (2000). (14) Dessauges-Zavadsky et al. (2006b). (15) Dessauges-Zavadsky et al. (2007). (16) Rafelski et al. (2012). (17) Herbert-Fort et al. (2006). (18) Ellison et al. (2010b). (19) Krogager et al. (2013b).

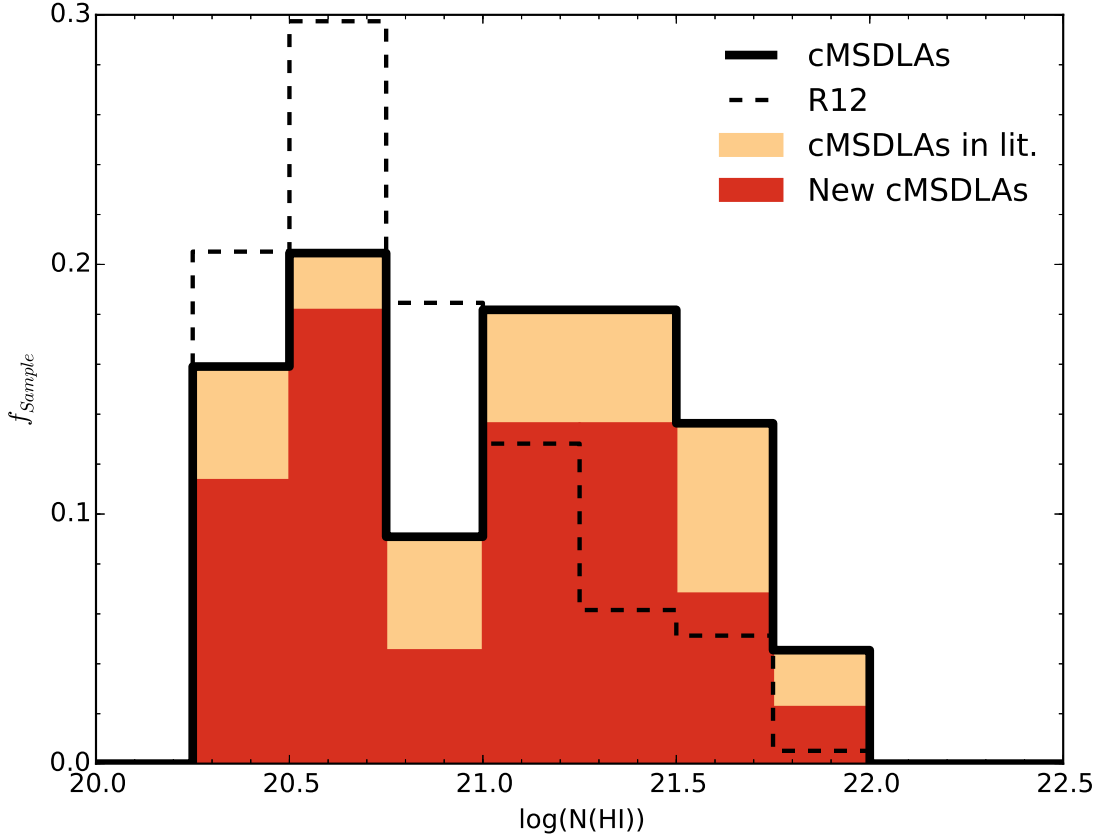


Fig. 33.— $N(\text{HI})$ distribution of the cMSDLA sample (solid black line) compared to the R12 literature DLAs (black dashed line). The darker shade represents the fraction of cMSDLAs observed in this work, while the lighter shade shows the contribution from cMSDLAs already observed in the literature. Although the cMSDLAs span the entire range of $N(\text{HI})$ values seen in the R12 DLAs; our sample is clearly biased towards systems with high HI column densities, with nearly half having an HI column density $\log N(\text{HI}) > 21$.

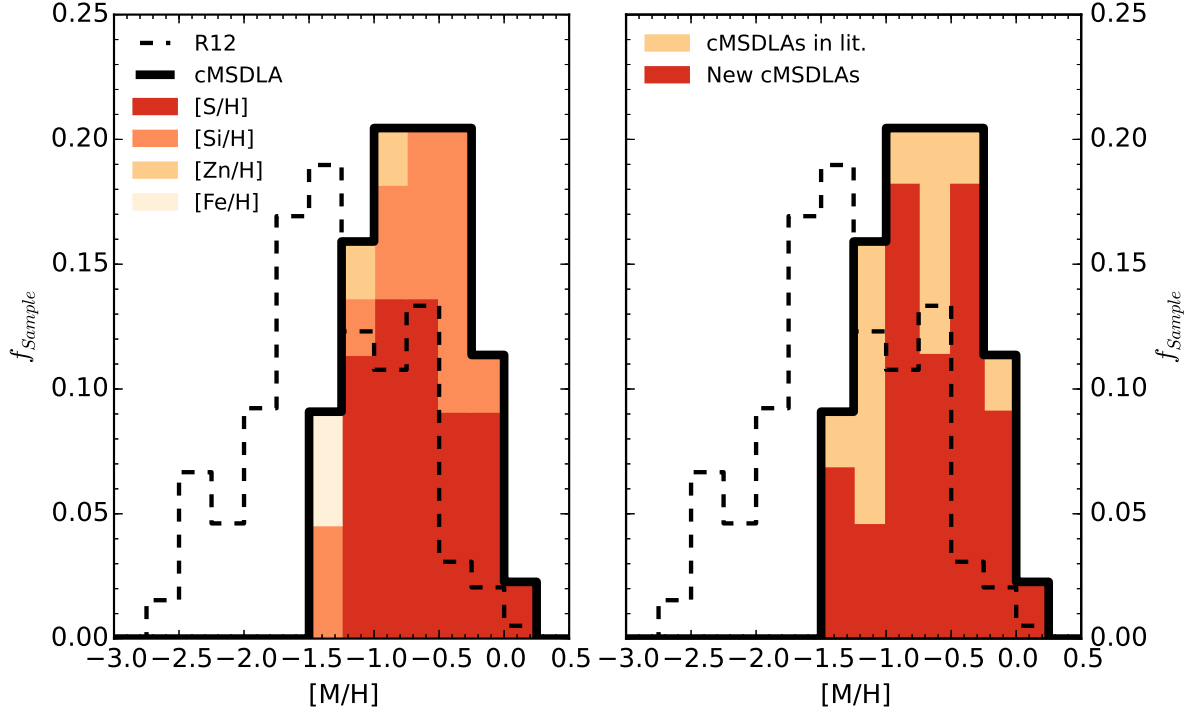


Fig. 34.— Metallicity distribution of the cMSDLA sample compared to the R12 DLA sample (black dashed line). DLAs with limits on their metallicities are not shown. *Left panel:* The different shades divide the distribution into fractions of which elements were used as a metallicity indicator in each bin. It is clear that cMSDLA sample probes a higher metallicity range than the DLAs from the R12 sample (median $[M/H] \sim -0.7$ dex compared to ~ -1.5 dex in the R12 sample). Sulphur is the dominant metallicity tracer adopted at higher metallicities (whereas silicon is the most used metallicity tracer in R12) as it is more likely reliably detected with higher column densities. *Right panel:* The distribution is separated into the 13 cMSDLAs from the literature and the 31 new cMSDLAs, following the same shading scheme in Figure 33.

observations without the atmospheric cutoffs of HIRES and SDSS (HF06; Adelman-McCarthy et al. 2008). However, our cMSDLA sample probes the most metal-rich systems (compared to the R12 literature) for the redshifts in which they are observed.

With the measured column densities from the previous section (Table 4), the cMSDLA sample can be classified into bona fide MSDLAs or not. Using the column density cuts $\log N(\text{SiII}) \geq 15.95$ or $\log N(\text{ZnII}) \geq 13.15$ from HF06, 20 of our cMSDLA sample are truly MSDLAs, while the other 24 do not satisfy the requirements (presented in Table 5). To highlight the number of DLAs that are true MSDLAs, Figure 36 shows the distribution of column density distributions for SiII (left panel) and ZnII (right panel). For all DLAs in the R12 literature sample, only 6.6% of DLAs make the MSDLA cut. The rarity of bona fide MSDLAs observed indicates that the column density cuts are targeting a very unique sample of DLAs.

It is interesting to note that there is little distinction between the metallicity distribution of bona fide MSDLAs and the DLAs from our sample that do not make the HF06 column density cuts, as inferred by their high $N(\text{HI})$ and metal columns. In addition, other than in FJ0812+3208 (for which the HF06 MSDLA classification was defined), the only other $> 3\sigma$ detection of boron comes from a DLA that does not make the MSDLA cut defined in HF06 (Berg et al. 2013). This suggests that the HF06 MSDLA classification scheme may be too strict for defining the optimal sample to study the nucleosynthesis of the most evolved galaxies at this epoch. The dashed-dotted line in Figure 36 demonstrates that taking an arbitrary cut of the top 10% of metal columns in the R12 literature sample ($\log N(\text{Si}) > 15.60$; $\log N(\text{Zn}) > 13.15^8$) can still provide an appropriate sample for the study of the most metal-rich systems in the early universe, despite not being true MSDLAs. We therefore do not further differentiate our cMSDLA sample between bona fide MSDLAs and DLAs that do not make the HF06 metal column density cuts, as we have demonstrated both types of DLAs are metal-rich (Figure 34) and have probed the highest metal column density systems (Figure 36). Such a differentiation would have no overall effect to the science goals of (i) searching for exotic elements in DLAs to provide nucleosynthetic constraints in the early universe, and (ii) compare the chemistry of DLAs to the higher metallicity components of the Milky Way (i.e. the thin and thick disk).

⁸Note that of the R12 literature DLAs where ZnII is detected, the 90th percentile nearly corresponds with the MSDLA cut in $\log N(\text{Zn}) = 13.15$. However, only 94 of the 260 R12 DLAs have a measured $N(\text{Zn})$. As zinc is a relatively rare element (Asplund et al. 2009) and the $\text{ZnII}\lambda 2026$ used for obtaining column densities is a naturally weak line, it is likely that these 94 systems are biased towards higher metal column densities where zinc can be detected. Therefore this 90th percentile $\log N(\text{Zn})$ cut is not representative of a general DLA distribution, and should be taken as an upper limit.

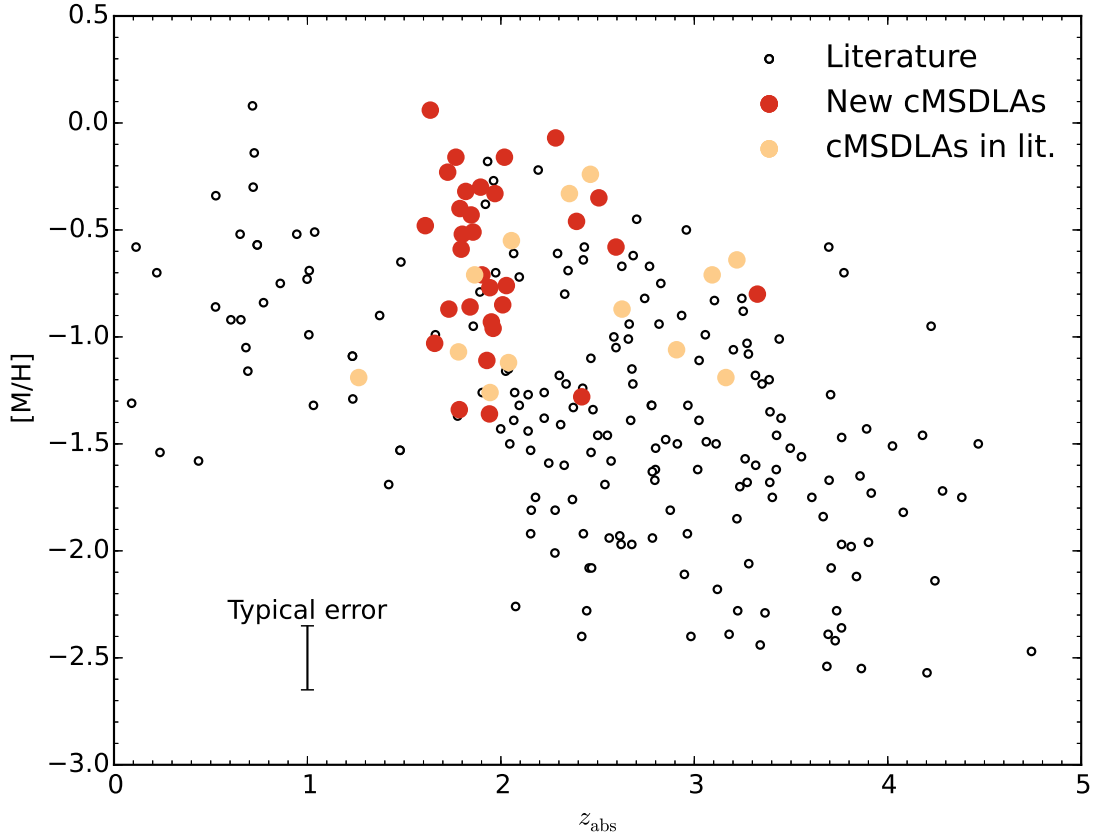


Fig. 35.— cMSDLA sample metallicity as a function of z_{abs} . The R12 sample DLAs are represented by the smaller unfilled circles, while the larger filled circles show the cMSDLA sample (darker shaded circles for the new cMSDLAs; lighter shaded circles for cMSDLAs taken from the literature). It is clear that the cMSDLA sample probes the highest metallicity DLAs within the redshift range of $1.5 \lesssim z_{\text{abs}} \lesssim 3.5$.

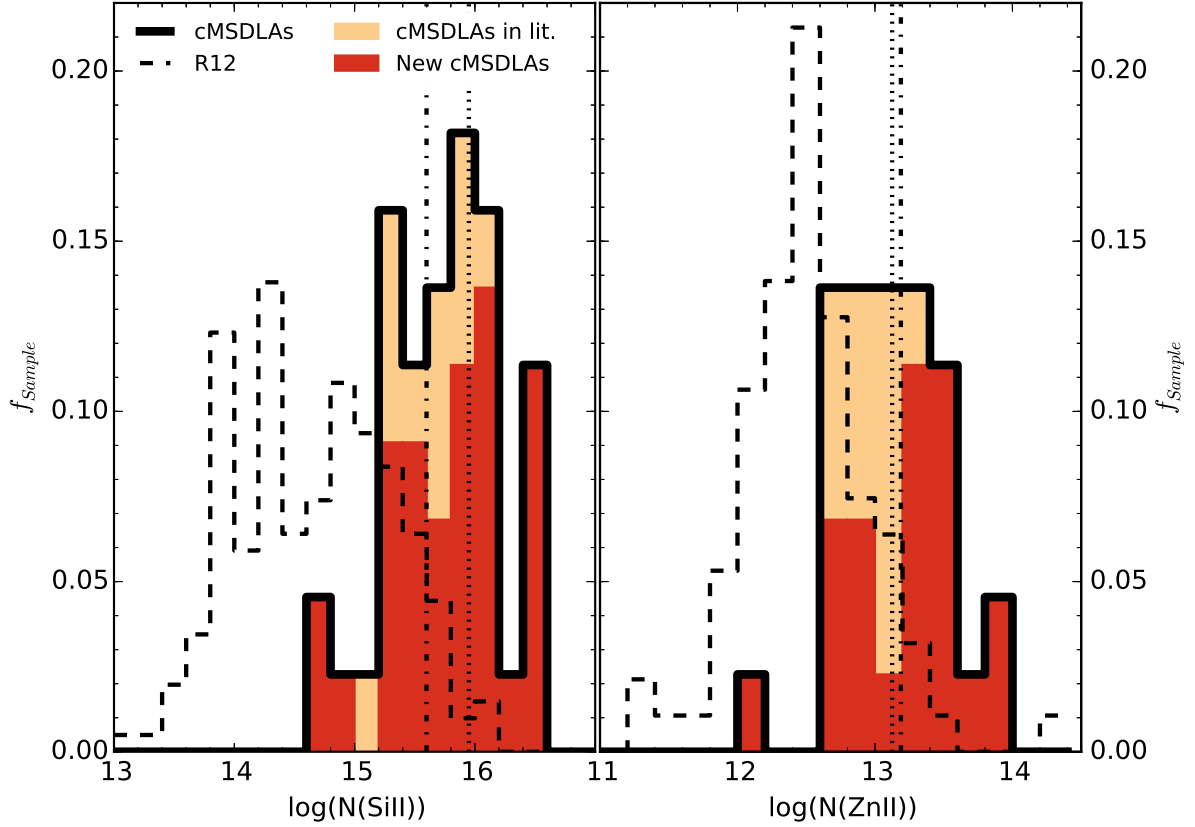


Fig. 36.— Column density distributions of SiII (*left panel*) and ZnII (*right panel*) for both the cMSDLAs and DLAs within the R12 literature (following the same notation as in Figure 33). The MSDLA column density limits ($N(\text{SiII}) \geq 15.95$; $N(\text{ZnII}) \geq 13.15$) are shown as the vertical dotted lines in each panel. Only $\sim 6\%$ of DLAs observed in the R12 literature appear to be genuine MSDLAs; while $\sim 45\%$ of the cMSDLA sample makes the HF06 column cut. Selecting the 90th percentile of the R12 column density distributions (dotted-dashed lines) selects the majority of the cMSDLA sample. The 90th percentile cut for $\log N(\text{Zn})$ is nearly equivalent to the MSDLA column cut. For clarity, the two vertical lines in the right hand panel representing these column density cuts have been separated by 0.05 dex.

4.2. Concluding Remarks

In this paper we have added high resolution observations of an additional 31 candidate MSDLAs to a pre-existing sample of 13 systems. Our 44 system sample of metal-rich DLAs spans the entire range of HI column densities seen in the R12 literature (although our sample is biased to higher $N(\text{HI})$ systems), and probes the higher end of the metallicity distribution of DLAs at redshifts > 1.5 . Furthermore, MSDLAs are very rare, accounting for only $\sim 6\%$ of all systems observed with high resolution spectrographs in the literature. However, we see little evidence for a fundamental difference between our DLA sample and DLAs that meet the subjective HF06 cut. We find that our entire sample remains useful for probing the top 10% of metal column densities of DLAs ($\log N(\text{Si}) > 15.60$; $\log N(\text{Zn}) > 13.15$). With the typical redshift of our sample being at $z \sim 2$, we are probing galactic chemical enrichment at times when the universe was only ~ 3 Gyr old. As we will discuss in a forthcoming paper (Paper II), we can get a better understanding of chemical evolution history of DLAs in comparison to the different chemical regimes of the Milky Way system using this metal-rich DLA sample as they are nearly as enriched as the Milky Way already at $z \sim 2$.

Acknowledgments

We dedicate this paper in memory of A. M. Wolfe. We thank Marc Rafelski for providing us with the $N(\text{Si})$ and $N(\text{Zn})$ from his literature sample, and the anonymous referee for their useful comments on improving the manuscript. MN and JXP are partially supported by NSF grant AST-1109452. We wish to recognize and acknowledge the very significant cultural role and reverence that the summit of Mauna Kea has always had within the indigenous Hawaiian community. We are most fortunate to have the opportunity to conduct observations from this mountain. The data presented herein were obtained at the W.M. Keck Observatory, which is operated as a scientific partnership among the California Institute of Technology, the University of California and the National Aeronautics and Space Administration. The Observatory was made possible by the generous financial support of the W.M. Keck Foundation.

REFERENCES

- Adelman-McCarthy, J. K., Agüeros, M. A., Allam, S. S., et al. 2008, *ApJS*, 175, 297
- Akerman, C. J., Ellison, S. L., Pettini, M., & Steidel, C. C. 2005, *A&A*, 440, 499
- Asplund, M., Grevesse, N., Sauval, A. J., & Scott, P. 2009, *ARA&A*, 47, 481
- Battisti, A. J., Meiring, J. D., Tripp, T. M., et al. 2012, *ApJ*, 744, 93
- Berg, T. A. M., Ellison, S. L., Venn, K. A., & Prochaska, J. X. 2013, *MNRAS*, 434, 2892

- Christensen, L., Møller, P., Fynbo, J. P. U., & Zafar, T. 2014, *MNRAS*, 445, 225
- Cooke, R., Pettini, M., & Jorgenson, R. A. 2014, *ArXiv e-prints*, arXiv:1406.7003
- Cooke, R., Pettini, M., Steidel, C. C., Rudie, G. C., & Nissen, P. E. 2011, *MNRAS*, 417, 1534
- Dessauges-Zavadsky, M., Calura, F., Prochaska, J. X., D’Odorico, S., & Matteucci, F. 2004, *A&A*, 416, 79
- . 2007, *A&A*, 470, 431
- Dessauges-Zavadsky, M., Prochaska, J. X., D’Odorico, S., Calura, F., & Matteucci, F. 2006a, *A&A*, 445, 93
- . 2006b, *A&A*, 445, 93
- Edvardsson, B., Andersen, J., Gustafsson, B., et al. 1993, *A&AS*, 102, 603
- Ellison, S. L., Kanekar, N., Prochaska, J. X., Momjian, E., & Worseck, G. 2012, *MNRAS*, 424, 293
- Ellison, S. L., Prochaska, J. X., Hennawi, J., et al. 2010a, *MNRAS*, 406, 1435
- . 2010b, *MNRAS*, 406, 1435
- Ellison, S. L., Prochaska, J. X., & Mendel, J. T. 2011, *MNRAS*, 412, 448
- Ellison, S. L., Ryan, S. G., & Prochaska, J. X. 2001, *MNRAS*, 326, 628
- Fynbo, J. P. U., Geier, S. J., Christensen, L., et al. 2013, *MNRAS*, 436, 361
- Haehnelt, M. G., Steinmetz, M., & Rauch, M. 1998, *ApJ*, 495, 647
- Herbert-Fort, S., Prochaska, J. X., Dessauges-Zavadsky, M., et al. 2006, *PASP*, 118, 1077
- Jorgenson, R. A., Wolfe, A. M., & Prochaska, J. X. 2010, *ApJ*, 722, 460
- Kanekar, N., Prochaska, J. X., Smette, A., et al. 2014, *MNRAS*, 438, 2131
- Kaplan, K. F., Prochaska, J. X., Herbert-Fort, S., Ellison, S. L., & Dessauges-Zavadsky, M. 2010, *PASP*, 122, 619
- Krogager, J.-K., Fynbo, J. P. U., Ledoux, C., et al. 2013a, *MNRAS*, arXiv:1304.4231
- . 2013b, *MNRAS*, 433, 3091
- Ledoux, C., Bergeron, J., & Petitjean, P. 2002, *A&A*, 385, 802
- Ledoux, C., Petitjean, P., Fynbo, J. P. U., Møller, P., & Srianand, R. 2006, *A&A*, 457, 71
- Ledoux, C., Petitjean, P., & Srianand, R. 2003, *MNRAS*, 346, 209

- Lopez, S., & Ellison, S. L. 2003, *A&A*, 403, 573
- Lu, L., Sargent, W. L. W., Barlow, T. A., Churchill, C. W., & Vogt, S. S. 1996, *ApJS*, 107, 475
- Meiring, J. D., Kulkarni, V. P., Khare, P., et al. 2006, *MNRAS*, 370, 43
- Milutinovic, N., Ellison, S. L., Prochaska, J. X., & Tumlinson, J. 2010, *MNRAS*, 408, 2071
- Morton, D. C. 2003, *ApJS*, 149, 205
- Neeleman, M., Wolfe, A. M., Prochaska, J. X., & Rafelski, M. 2013, *ApJ*, 769, 54
- Nestor, D. B., Pettini, M., Hewett, P. C., Rao, S., & Wild, V. 2008, *MNRAS*, 390, 1670
- Noterdaeme, P., Petitjean, P., Carithers, W. C., et al. 2012, *A&A*, 547, L1
- Penprase, B. E., Prochaska, J. X., Sargent, W. L. W., Toro-Martinez, I., & Beeler, D. J. 2010, *ApJ*, 721, 1
- Petitjean, P., Srianand, R., & Ledoux, C. 2000, *A&A*, 364, L26
- Pettini, M., Boksenberg, A., & Hunstead, R. W. 1990, *ApJ*, 348, 48
- Pettini, M., Ellison, S. L., Steidel, C. C., Shapley, A. E., & Bowen, D. V. 2000, *ApJ*, 532, 65
- Pettini, M., Smith, L. J., Hunstead, R. W., & King, D. L. 1994, *ApJ*, 426, 79
- Pettini, M., Smith, L. J., King, D. L., & Hunstead, R. W. 1997, *ApJ*, 486, 665
- Prochaska, J. X., Gawiser, E., & Wolfe, A. M. 2001a, *ApJ*, 552, 99
- Prochaska, J. X., Gawiser, E., Wolfe, A. M., Castro, S., & Djorgovski, S. G. 2003a, *ApJ*, 595, L9
- Prochaska, J. X., Gawiser, E., Wolfe, A. M., Cooke, J., & Gelino, D. 2003b, *ApJS*, 147, 227
- Prochaska, J. X., Hennawi, J. F., & Herbert-Fort, S. 2008, *ApJ*, 675, 1002
- Prochaska, J. X., Henry, R. B. C., O’Meara, J. M., et al. 2002, *PASP*, 114, 933
- Prochaska, J. X., & Herbert-Fort, S. 2004, *PASP*, 116, 622
- Prochaska, J. X., Herbert-Fort, S., & Wolfe, A. M. 2005, *ApJ*, 635, 123
- Prochaska, J. X., Howk, J. C., & Wolfe, A. M. 2003c, *Nature*, 423, 57
- Prochaska, J. X., & Wolfe, A. M. 1996, *ApJ*, 470, 403
- . 1997, *ApJ*, 487, 73
- . 1999, *ApJS*, 121, 369

- . 2002, *ApJ*, 566, 68
- Prochaska, J. X., Wolfe, A. M., Howk, J. C., et al. 2007, *ApJS*, 171, 29
- Prochaska, J. X., Wolfe, A. M., Tytler, D., et al. 2001b, *ApJS*, 137, 21
- . 2001c, *ApJS*, 137, 21
- Rafelski, M., Wolfe, A. M., Prochaska, J. X., Neeleman, M., & Mendez, A. J. 2012, *ApJ*, 755, 89
- Savage, B. D., & Sembach, K. R. 1991, *ApJ*, 379, 245
- Sheinis, A. I., Bolte, M., Epps, H. W., et al. 2002, *PASP*, 114, 851
- Srianand, R., Noterdaeme, P., Ledoux, C., & Petitjean, P. 2008, *A&A*, 482, L39
- Srianand, R., Petitjean, P., Ledoux, C., Ferland, G., & Shaw, G. 2005, *MNRAS*, 362, 549
- Suzuki, N., Tytler, D., Kirkman, D., O’Meara, J. M., & Lubin, D. 2003, *PASP*, 115, 1050
- Tumlinson, J., Malec, A. L., Carswell, R. F., et al. 2010, *ApJ*, 718, L156
- Vladilo, G., Abate, C., Yin, J., Cescutti, G., & Matteucci, F. 2011, *A&A*, 530, A33
- Vogt, S. S., Allen, S. L., Bigelow, B. C., et al. 1994, in *Society of Photo-Optical Instrumentation Engineers (SPIE) Conference Series*, Vol. 2198, *Instrumentation in Astronomy VIII*, ed. D. L. Crawford & E. R. Craine, 362
- Wolfe, A. M., Lanzetta, K. M., Foltz, C. B., & Chaffee, F. H. 1995, *ApJ*, 454, 698
- Wolfe, A. M., Prochaska, J. X., Jorgenson, R. A., & Rafelski, M. 2008, *ApJ*, 681, 881
- Wolfe, A. M., Turnshek, D. A., Smith, H. E., & Cohen, R. D. 1986, *ApJS*, 61, 249
- York, B. A., Kanekar, N., Ellison, S. L., & Pettini, M. 2007, *MNRAS*, 382, L53
- Zafar, T., Centurión, M., Péroux, C., et al. 2014a, *MNRAS*, 444, 744
- Zafar, T., Vladilo, G., Péroux, C., et al. 2014b, *ArXiv e-prints*, arXiv:1409.4577

A. Additional Material

Table A.1: Metal column densities for J0008–0958 ($z_{\text{abs}}=1.77$)

Ion	Line	λ Å	f	v_{min} km s ⁻¹	v_{max} km s ⁻¹	logN(X)	Included	logN _{adopt}
SiII	1260	1260.422	1.01×10^0	-245	150	> 14.51	N	
SiII	1304	1304.370	9.40×10^{-2}	-245	150	> 15.38	N	
SiII	1526	1526.707	1.27×10^{-1}	-245	150	> 15.22	N	
SiII	1808	1808.013	2.19×10^{-3}	-245	150	16.04 ± 0.05	Y	
SiII	–	–	–	–	–	–	–	16.04 ± 0.05
SII	1250	1250.584	5.43×10^{-3}	-245	150	15.84 ± 0.05	Y	
SII	1253	1253.811	1.09×10^{-2}	-245	150	> 16.01	N	
SII	–	–	–	–	–	–	–	15.84 ± 0.05
CrII	2056	2056.254	1.05×10^{-1}	-245	150	13.92 ± 0.05	Y	
CrII	2066	2066.161	5.15×10^{-2}	-245	150	13.86 ± 0.05	Y	
CrII	–	–	–	–	–	–	–	13.91 ± 0.05
FeII	1608	1608.451	5.80×10^{-2}	-245	150	> 15.38	N	
FeII	1611	1611.200	1.36×10^{-3}	-245	150	15.62 ± 0.05	Y	
FeII	–	–	–	–	–	–	–	15.62 ± 0.05
NiII	1317	1317.217	5.71×10^{-2}	-245	150	14.50 ± 0.05	Y	
NiII	1370	1370.131	5.88×10^{-2}	-245	150	14.41 ± 0.05	Y	
NiII	1454	1454.842	3.23×10^{-2}	-245	150	14.43 ± 0.05	Y	
NiII	1703	1703.405	6.00×10^{-3}	-245	150	14.26 ± 0.12	Y	
NiII	1709	1709.604	3.24×10^{-2}	-245	150	14.35 ± 0.05	Y	
NiII	1741	1741.553	4.27×10^{-2}	-245	150	14.45 ± 0.05	Y	
NiII	1751	1751.916	2.77×10^{-2}	-245	150	14.55 ± 0.05	Y	
NiII	–	–	–	–	–	–	–	14.46 ± 0.05
ZnII	2026	2026.136	4.89×10^{-1}	-245	150	13.31 ± 0.05	Y	
ZnII	2062	2062.664	2.56×10^{-1}	-245	250	13.51 ± 0.05	N	
ZnII	–	–	–	–	–	–	–	13.31 ± 0.05

Table A.3: Metal column densities for J0058+0115 ($z_{\text{abs}}=2.01$)

Ion	Line	λ \AA	f	v_{min} km s^{-1}	v_{max} km s^{-1}	$\log N(X)$	Included	$\log N_{\text{adopt}}$
SiII	1260	1260.422	1.01×10^0	−90	400	> 14.47	N	
SiII	1304	1304.370	9.40×10^{-2}	−90	400	> 15.29	Y	
SiII	1526	1526.707	1.27×10^{-1}	−90	400	> 15.16	Y	
SiII	1808	1808.013	2.19×10^{-3}	−90	80	> 15.55	Y	
SiII	–	–	–	–	–	–	–	> 15.55
SII	1253	1253.811	1.09×10^{-2}	−90	400	15.40 ± 0.05	Y	
SII	–	–	–	–	–	–	–	15.40 ± 0.05
CrII	2056	2056.254	1.05×10^{-1}	−60	300	13.54 ± 0.05	Y	
CrII	–	–	–	–	–	–	–	13.54 ± 0.05
FeII	1608	1608.451	5.80×10^{-2}	−90	400	> 15.19	N	
FeII	1611	1611.200	1.36×10^{-3}	−90	400	15.18 ± 0.05	Y	
FeII	–	–	–	–	–	–	–	15.18 ± 0.05
NiII	1709	1709.604	3.24×10^{-2}	−90	400	14.10 ± 0.05	Y	
NiII	1741	1741.553	4.27×10^{-2}	−90	400	14.19 ± 0.05	Y	
NiII	1751	1751.916	2.77×10^{-2}	−90	400	14.07 ± 0.06	Y	
NiII	–	–	–	–	–	–	–	14.16 ± 0.05
ZnII	2026	2026.136	4.89×10^{-1}	−60	400	12.95 ± 0.05	Y	
ZnII	–	–	–	–	–	–	–	12.95 ± 0.05

Table A.4: Metal column densities for J0211+1241 ($z_{\text{abs}}=2.60$)

Ion	Line	λ \AA	f	v_{min} km s^{-1}	v_{max} km s^{-1}	$\log N(X)$	Included	$\log N_{\text{adopt}}$
SiII	1526	1526.707	1.27×10^{-1}	−470	90	> 14.89	Y	
SiII	1808	1808.013	2.19×10^{-3}	−470	90	15.53 ± 0.08	Y	
SiII	–	–	–	–	–	–	–	15.53 ± 0.08
FeII	1143	1143.226	1.77×10^{-2}	−80	40	15.06 ± 0.05	Y	
FeII	1608	1608.451	5.80×10^{-2}	−470	90	> 14.90	Y	
FeII	1611	1611.200	1.36×10^{-3}	−470	90	< 16.05	Y	
FeII	–	–	–	–	–	–	–	15.06 ± 0.05
NiII	1709	1709.604	3.24×10^{-2}	−470	90	14.07 ± 0.06	Y	
NiII	1741	1741.553	4.27×10^{-2}	−470	90	14.06 ± 0.10	Y	
NiII	1751	1751.916	2.77×10^{-2}	−470	90	< 14.25	N	
NiII	–	–	–	–	–	–	–	14.07 ± 0.05

Table A.5: Metal column densities for J0233+0103 ($z_{\text{abs}}=1.78$)

Ion	Line	λ Å	f	v_{min} km s ⁻¹	v_{max} km s ⁻¹	logN(X)	Included	logN _{adopt}
SiII	1304	1304.370	9.40×10^{-2}	-100	60	> 14.78	Y	
SiII	1526	1526.707	1.27×10^{-1}	-100	60	> 14.69	Y	
SiII	1808	1808.013	2.19×10^{-3}	-100	60	< 14.76	Y	
SiII	–	–	–	–	–	–	–	14.77 ± 0.05
FeII	1608	1608.451	5.80×10^{-2}	-100	60	14.62 ± 0.05	Y	
FeII	–	–	–	–	–	–	–	14.62 ± 0.05
NiII	1741	1741.553	4.27×10^{-2}	-100	60	13.61 ± 0.11	Y	
NiII	–	–	–	–	–	–	–	13.61 ± 0.11

Table A.6: Metal column densities for J0815+1037 ($z_{\text{abs}}=1.85$)

Ion	Line	λ Å	f	v_{min} km s ⁻¹	v_{max} km s ⁻¹	logN(X)	Included	logN _{adopt}
SiII	1304	1304.370	9.40×10^{-2}	-200	100	> 14.95	Y	
SiII	1526	1526.707	1.27×10^{-1}	-200	100	> 14.73	Y	
SiII	1808	1808.013	2.19×10^{-3}	-200	100	15.38 ± 0.45	Y	
SiII	–	–	–	–	–	–	–	15.38 ± 0.45
FeII	1608	1608.451	5.80×10^{-2}	-200	100	> 14.87	Y	
FeII	–	–	–	–	–	–	–	> 14.87
NiII	1317	1317.217	5.71×10^{-2}	-50	50	13.74 ± 0.12	Y	
NiII	–	–	–	–	–	–	–	13.74 ± 0.12

Table A.7: Metal column densities for J0927+1543 ($z_{\text{abs}}=1.73$)

Ion	Line	λ \AA	f	v_{min} km s^{-1}	v_{max} km s^{-1}	$\log N(X)$	Included	$\log N_{\text{adopt}}$
SiII	1304	1304.370	9.40×10^{-2}	-230	190	> 15.27	N	
SiII	1526	1526.707	1.27×10^{-1}	-230	190	> 15.14	N	
SiII	1808	1808.013	2.19×10^{-3}	-230	190	15.99 ± 0.05	Y	
SiII	–	–	–	–	–	–	–	15.99 ± 0.05
CrII	2056	2056.254	1.05×10^{-1}	-230	190	13.86 ± 0.05	Y	
CrII	2066	2066.161	5.15×10^{-2}	-230	190	13.76 ± 0.09	Y	
CrII	–	–	–	–	–	–	–	13.83 ± 0.05
FeII	1608	1608.451	5.80×10^{-2}	-230	190	> 15.17	Y	
FeII	1611	1611.200	1.36×10^{-3}	-230	190	< 15.13	Y	
FeII	–	–	–	–	–	–	–	15.14 ± 0.24
NiII	1709	1709.604	3.24×10^{-2}	-230	190	14.04 ± 0.09	Y	
NiII	1741	1741.553	4.27×10^{-2}	-230	190	14.19 ± 0.05	Y	
NiII	1751	1751.916	2.77×10^{-2}	-230	190	14.26 ± 0.06	Y	
NiII	–	–	–	–	–	–	–	14.17 ± 0.05
ZnII	2026	2026.136	4.89×10^{-1}	-230	190	< 13.69	Y	
ZnII	2062	2062.664	2.56×10^{-1}	-230	190	13.38 ± 0.05	Y	
ZnII	–	–	–	–	–	–	–	13.38 ± 0.05

Table A.8: Metal column densities for J0927+5823 ($z_{\text{abs}}=1.64$)

Ion	Line	λ Å	f	v_{min} km s ⁻¹	v_{max} km s ⁻¹	logN(X)	Included	logN _{adopt}
SiII	1526	1526.707	1.27×10^{-1}	-255	255	> 15.24	N	
SiII	1808	1808.013	2.19×10^{-3}	-255	255	15.72 ± 0.05	Y	
SiII	–	–	–	–	–	–	–	15.72 ± 0.05
SII	1250	1250.584	5.43×10^{-3}	-130	180	15.61 ± 0.05	Y	
SII	–	–	–	–	–	–	–	15.61 ± 0.05
CrII	2056	2056.254	1.05×10^{-1}	-130	255	13.55 ± 0.05	N	
CrII	–	–	–	–	–	–	–	...
FeII	1608	1608.451	5.80×10^{-2}	-255	255	> 15.27	Y	
FeII	1611	1611.200	1.36×10^{-3}	-255	255	< 14.95	Y	
FeII	–	–	–	–	–	–	–	> 15.27
NiII	1317	1317.217	5.71×10^{-2}	-255	255	14.45 ± 0.05	Y	
NiII	1454	1454.842	3.23×10^{-2}	-255	255	14.45 ± 0.05	Y	
NiII	1709	1709.604	3.24×10^{-2}	-255	255	14.46 ± 0.05	Y	
NiII	1741	1741.553	4.27×10^{-2}	-255	255	14.42 ± 0.05	Y	
NiII	–	–	–	–	–	–	–	14.44 ± 0.05
ZnII	2026	2026.136	4.89×10^{-1}	-130	180	13.27 ± 0.05	Y	
ZnII	2062	2062.664	2.56×10^{-1}	-130	130	13.38 ± 0.05	Y	
ZnII	–	–	–	–	–	–	–	13.29 ± 0.05

Table A.10: Metal column densities for J1013+5615 ($z_{\text{abs}}=2.28$)

Ion	Line	λ Å	f	v_{min} km s ⁻¹	v_{max} km s ⁻¹	logN(X)	Included	logN _{adopt}
SiII	1526	1526.707	1.27×10^{-1}	-140	185	> 15.21	N	
SiII	1808	1808.013	2.19×10^{-3}	-140	175	16.14 ± 0.05	Y	
SiII	–	–	–	–	–	–	–	16.14 ± 0.05
CrII	2056	2056.254	1.05×10^{-1}	-140	175	13.80 ± 0.05	Y	
CrII	2066	2066.161	5.15×10^{-2}	-140	175	13.66 ± 0.08	Y	
CrII	–	–	–	–	–	–	–	13.79 ± 0.05
FeII	1608	1608.451	5.80×10^{-2}	-140	175	> 15.44	Y	
FeII	–	–	–	–	–	–	–	> 15.45
ZnII	2026	2026.136	4.89×10^{-1}	-140	175	13.56 ± 0.05	Y	
ZnII	–	–	–	–	–	–	–	13.56 ± 0.05

Table A.11: Metal column densities for J1024+0600 ($z_{\text{abs}}=1.90$)

Ion	Line	λ Å	f	v_{min} km s ⁻¹	v_{max} km s ⁻¹	logN(X)	Included	logN _{adopt}
SiII	1304	1304.370	9.40×10^{-2}	-250	220	> 15.33	N	
SiII	1526	1526.707	1.27×10^{-1}	-250	220	> 15.19	N	
SiII	1808	1808.013	2.19×10^{-3}	-90	160	15.81 ± 0.05	Y	
SiII	–	–	–	–	–	–	–	15.81 ± 0.05
SII	1250	1250.584	5.43×10^{-3}	-60	160	15.42 ± 0.05	Y	
SII	1253	1253.811	1.09×10^{-2}	-60	160	15.47 ± 0.05	Y	
SII	–	–	–	–	–	–	–	15.45 ± 0.05
FeII	1608	1608.451	5.80×10^{-2}	-250	160	> 15.21	N	
FeII	1611	1611.200	1.36×10^{-3}	-60	50	15.27 ± 0.08	Y	
FeII	–	–	–	–	–	–	–	15.27 ± 0.08
NiII	1317	1317.217	5.71×10^{-2}	-60	140	13.93 ± 0.05	Y	
NiII	1370	1370.131	5.88×10^{-2}	-60	160	14.06 ± 0.05	Y	
NiII	1709	1709.604	3.24×10^{-2}	-60	160	14.26 ± 0.05	Y	
NiII	1741	1741.553	4.27×10^{-2}	-60	160	14.20 ± 0.05	Y	
NiII	–	–	–	–	–	–	–	14.02 ± 0.05

Table A.13: Metal column densities for J1049–0110 ($z_{\text{abs}}=1.66$)

Ion	Line	λ Å	f	v_{min} km s ⁻¹	v_{max} km s ⁻¹	logN(X)	Included	logN _{adopt}
SiII	1304	1304.370	9.40×10^{-2}	-190	400	> 15.38	N	
SiII	1526	1526.707	1.27×10^{-1}	-190	400	> 15.24	Y	
SiII	1808	1808.013	2.19×10^{-3}	-190	400	15.80 ± 0.05	Y	
SiII	–	–	–	–	–	–	–	15.80 ± 0.05
SII	1250	1250.584	5.43×10^{-3}	-10	400	< 15.47	N	
SII	1253	1253.811	1.09×10^{-2}	-190	400	15.47 ± 0.05	Y	
SII	–	–	–	–	–	–	–	15.47 ± 0.05
CrII	2056	2056.254	1.05×10^{-1}	-70	400	13.48 ± 0.05	Y	
CrII	2066	2066.161	5.15×10^{-2}	-100	200	13.51 ± 0.07	Y	
CrII	–	–	–	–	–	–	–	13.49 ± 0.05
FeII	1608	1608.451	5.80×10^{-2}	-190	400	> 15.15	N	
FeII	1611	1611.200	1.36×10^{-3}	-120	280	< 14.97	N	
FeII	2260	2260.780	2.44×10^{-3}	-90	200	15.17 ± 0.05	Y	
FeII	–	–	–	–	–	–	–	15.17 ± 0.05
NiII	1317	1317.217	5.71×10^{-2}	-70	300	14.29 ± 0.05	Y	
NiII	1454	1454.842	3.23×10^{-2}	-190	400	13.89 ± 0.08	Y	
NiII	1709	1709.604	3.24×10^{-2}	-190	400	14.38 ± 0.05	Y	
NiII	1741	1741.553	4.27×10^{-2}	-20	400	14.30 ± 0.05	Y	
NiII	1751	1751.916	2.77×10^{-2}	-190	400	14.16 ± 0.05	Y	
NiII	–	–	–	–	–	–	–	14.25 ± 0.05
ZnII	2026	2026.136	4.89×10^{-1}	-190	400	13.14 ± 0.05	Y	
ZnII	–	–	–	–	–	–	–	13.14 ± 0.05

Table A.14: Metal column densities for J1056+1208 ($z_{\text{abs}}=1.61$)

Ion	Line	λ Å	f	v_{min} km s ⁻¹	v_{max} km s ⁻¹	logN(X)	Included	logN _{adopt}
SiII	1304	1304.370	9.40×10^{-2}	-190	210	> 15.28	Y	
SiII	1526	1526.707	1.27×10^{-1}	-190	210	> 15.09	Y	
SiII	1808	1808.013	2.19×10^{-3}	-190	210	16.48 ± 0.09	Y	
SiII	–	–	–	–	–	–	–	16.48 ± 0.09
SII	1250	1250.584	5.43×10^{-3}	-190	210	> 16.15	Y	
SII	–	–	–	–	–	–	–	> 16.15
CrII	2056	2056.254	1.05×10^{-1}	-190	210	14.04 ± 0.05	Y	
CrII	2066	2066.161	5.15×10^{-2}	-190	210	14.02 ± 0.05	Y	
CrII	–	–	–	–	–	–	–	14.04 ± 0.05
FeII	1608	1608.451	5.80×10^{-2}	-190	210	> 15.23	N	
FeII	1611	1611.200	1.36×10^{-3}	-190	210	15.80 ± 0.05	Y	
FeII	2249	2249.877	1.82×10^{-3}	-190	210	15.79 ± 0.05	Y	
FeII	2260	2260.780	2.44×10^{-3}	-190	210	15.84 ± 0.05	Y	
FeII	–	–	–	–	–	–	–	15.81 ± 0.05
NiII	1317	1317.217	5.71×10^{-2}	-190	210	14.56 ± 0.05	Y	
NiII	1370	1370.131	5.88×10^{-2}	-190	210	14.61 ± 0.05	Y	
NiII	1454	1454.842	3.23×10^{-2}	-190	210	14.61 ± 0.05	Y	
NiII	1703	1703.405	6.00×10^{-3}	-190	210	14.64 ± 0.05	Y	
NiII	1709	1709.604	3.24×10^{-2}	-190	210	14.67 ± 0.05	Y	
NiII	1741	1741.553	4.27×10^{-2}	-190	210	14.78 ± 0.05	Y	
NiII	1751	1751.916	2.77×10^{-2}	-190	210	14.64 ± 0.05	Y	
NiII	–	–	–	–	–	–	–	14.69 ± 0.05
ZnII	2026	2026.136	4.89×10^{-1}	-190	210	13.76 ± 0.05	Y	
ZnII	–	–	–	–	–	–	–	13.76 ± 0.05

Table A.15: Metal column densities for J1106+1044 ($z_{\text{abs}}=1.82$)

Ion	Line	λ \AA	f	v_{min} km s^{-1}	v_{max} km s^{-1}	$\log N(X)$	Included	$\log N_{\text{adopt}}$
SiII	1304	1304.370	9.40×10^{-2}	-220	100	> 15.22	Y	
SiII	1526	1526.707	1.27×10^{-1}	-220	100	> 15.11	Y	
SiII	-	-	-	-	-	-	-	> 15.22
SiII	1250	1250.584	5.43×10^{-3}	-220	100	15.25 ± 0.05	Y	
SiII	1253	1253.811	1.09×10^{-2}	-220	100	15.35 ± 0.05	Y	
SiII	-	-	-	-	-	-	-	15.33 ± 0.05
FeII	1608	1608.451	5.80×10^{-2}	-220	100	> 15.15	Y	
FeII	1611	1611.200	1.36×10^{-3}	-220	100	< 15.16	Y	
FeII	-	-	-	-	-	-	-	> 15.15
NiII	1317	1317.217	5.71×10^{-2}	-220	100	14.06 ± 0.07	Y	
NiII	1709	1709.604	3.24×10^{-2}	-220	100	13.91 ± 0.12	Y	
NiII	1741	1741.553	4.27×10^{-2}	-220	100	14.04 ± 0.07	Y	
NiII	-	-	-	-	-	-	-	14.02 ± 0.05

Table A.16: Metal column densities for J1142+0701 ($z_{\text{abs}}=1.84$)

Ion	Line	λ Å	f	v_{min} km s ⁻¹	v_{max} km s ⁻¹	logN(X)	Included	logN _{adopt}
SiII	1304	1304.370	9.40×10^{-2}	-220	230	> 15.21	Y	
SiII	1526	1526.707	1.27×10^{-1}	-220	230	> 15.01	Y	
SiII	1808	1808.013	2.19×10^{-3}	-220	230	16.15 ± 0.13	Y	
SiII	–	–	–	–	–	–	–	16.15 ± 0.13
SII	1250	1250.584	5.43×10^{-3}	-200	40	> 15.69	N	
SII	1253	1253.811	1.09×10^{-2}	-200	40	> 15.52	N	
SII	–	–	–	–	–	–	–	...
CrII	2056	2056.254	1.05×10^{-1}	-110	40	13.74 ± 0.05	Y	
CrII	2062	2062.234	7.80×10^{-2}	-40	40	13.69 ± 0.05	Y	
CrII	2066	2066.161	5.15×10^{-2}	-40	40	13.63 ± 0.07	Y	
CrII	–	–	–	–	–	–	–	13.70 ± 0.05
FeII	1608	1608.451	5.80×10^{-2}	-220	230	> 15.09	N	
FeII	1611	1611.200	1.36×10^{-3}	-110	40	15.47 ± 0.05	Y	
FeII	–	–	–	–	–	–	–	15.47 ± 0.05
NiII	1317	1317.217	5.71×10^{-2}	-40	40	14.09 ± 0.05	Y	
NiII	1370	1370.131	5.88×10^{-2}	-40	40	14.11 ± 0.05	Y	
NiII	1454	1454.842	3.23×10^{-2}	-40	40	13.93 ± 0.08	N	
NiII	1709	1709.604	3.24×10^{-2}	-40	40	13.94 ± 0.05	Y	
NiII	1741	1741.553	4.27×10^{-2}	-40	40	13.96 ± 0.05	Y	
NiII	1751	1751.916	2.77×10^{-2}	-40	40	14.30 ± 0.05	N	
NiII	–	–	–	–	–	–	–	14.01 ± 0.05
ZnII	2026	2026.136	4.89×10^{-1}	-40	40	> 13.21	N	
ZnII	2062	2062.664	2.56×10^{-1}	-40	40	13.29 ± 0.05	Y	
ZnII	–	–	–	–	–	–	–	13.29 ± 0.05

Table A.17: Metal column densities for J1155+0530 ($z_{\text{abs}}=3.33$)

Ion	Line	λ Å	f	v_{min} km s ⁻¹	v_{max} km s ⁻¹	logN(X)	Included	logN _{adopt}
SiII	1304	1304.370	9.40×10^{-2}	-150	220	> 15.26	N	
SiII	1526	1526.707	1.27×10^{-1}	-150	220	> 15.08	N	
SiII	1808	1808.013	2.19×10^{-3}	-70	220	15.94 ± 0.05	Y	
SiII	–	–	–	–	–	–	–	15.94 ± 0.05
SII	1250	1250.584	5.43×10^{-3}	-70	220	15.61 ± 0.05	Y	
SII	1253	1253.811	1.09×10^{-2}	-60	190	15.35 ± 0.05	Y	
SII	–	–	–	–	–	–	–	15.40 ± 0.05
CrII	2066	2066.161	5.15×10^{-2}	-70	220	13.36 ± 0.09	Y	
CrII	–	–	–	–	–	–	–	13.36 ± 0.09
FeII	1608	1608.451	5.80×10^{-2}	-150	220	> 15.11	N	
FeII	1611	1611.200	1.36×10^{-3}	-70	160	15.37 ± 0.05	Y	
FeII	–	–	–	–	–	–	–	15.37 ± 0.05
NiII	1317	1317.217	5.71×10^{-2}	-70	220	13.95 ± 0.05	Y	
NiII	1370	1370.131	5.88×10^{-2}	-70	220	14.16 ± 0.05	Y	
NiII	1454	1454.842	3.23×10^{-2}	-70	220	14.09 ± 0.05	Y	
NiII	1709	1709.604	3.24×10^{-2}	-70	220	13.89 ± 0.05	Y	
NiII	1741	1741.553	4.27×10^{-2}	-70	220	14.01 ± 0.05	Y	
NiII	1751	1751.916	2.77×10^{-2}	-70	220	14.18 ± 0.05	Y	
NiII	–	–	–	–	–	–	–	14.07 ± 0.05
ZnII	2026	2026.136	4.89×10^{-1}	-70	220	12.89 ± 0.07	Y	
ZnII	–	–	–	–	–	–	–	12.89 ± 0.07

Table A.18: Metal column densities for J1305+0924 ($z_{\text{abs}}=2.02$)

Ion	Line	λ Å	f	v_{min} km s $^{-1}$	v_{max} km s $^{-1}$	logN(X)	Included	logN $_{\text{adopt}}$
SiII	1260	1260.422	1.01×10^0	–150	160	> 14.29	N	
SiII	1304	1304.370	9.40×10^{-2}	–150	160	> 15.14	N	
SiII	1808	1808.013	2.19×10^{-3}	–150	160	15.75 ± 0.05	Y	
SiII	–	–	–	–	–	–	–	15.75 ± 0.05
SII	1250	1250.584	5.43×10^{-3}	–150	160	15.45 ± 0.05	Y	
SII	1253	1253.811	1.09×10^{-2}	–150	160	15.39 ± 0.05	Y	
SII	1259	1259.519	1.66×10^{-2}	–150	75	15.36 ± 0.05	Y	
SII	–	–	–	–	–	–	–	15.39 ± 0.05
FeII	1608	1608.451	5.80×10^{-2}	–150	160	> 15.10	N	
FeII	1611	1611.200	1.36×10^{-3}	–50	40	15.21 ± 0.14	Y	
FeII	–	–	–	–	–	–	–	15.21 ± 0.14
NiII	1317	1317.217	5.71×10^{-2}	–150	160	14.31 ± 0.05	Y	
NiII	1709	1709.604	3.24×10^{-2}	–150	160	14.57 ± 0.05	Y	
NiII	1741	1741.553	4.27×10^{-2}	–150	160	14.28 ± 0.06	Y	
NiII	–	–	–	–	–	–	–	14.36 ± 0.05

Table A.19: Metal column densities for J1310+5424 ($z_{\text{abs}}=1.80$)

Ion	Line	λ Å	f	v_{min} km s ⁻¹	v_{max} km s ⁻¹	logN(X)	Included	logN _{adopt}
SiII	1260	1260.422	1.01×10^0	-110	60	> 14.10	N	
SiII	1304	1304.370	9.40×10^{-2}	-100	100	> 15.13	Y	
SiII	1526	1526.707	1.27×10^{-1}	-100	100	> 14.95	Y	
SiII	1808	1808.013	2.19×10^{-3}	-100	100	16.44 ± 0.05	Y	
SiII	–	–	–	–	–	–	–	16.44 ± 0.05
SII	1250	1250.584	5.43×10^{-3}	-80	90	> 16.05	Y	
SII	1253	1253.811	1.09×10^{-2}	-80	60	> 15.84	Y	
SII	–	–	–	–	–	–	–	> 16.05
CrII	2066	2066.161	5.15×10^{-2}	-60	80	13.99 ± 0.05	Y	
CrII	–	–	–	–	–	–	–	13.99 ± 0.05
FeII	1608	1608.451	5.80×10^{-2}	-100	80	> 15.10	Y	
FeII	1611	1611.200	1.36×10^{-3}	-60	90	15.64 ± 0.05	Y	
FeII	–	–	–	–	–	–	–	15.64 ± 0.05
NiII	1317	1317.217	5.71×10^{-2}	-60	90	14.44 ± 0.05	Y	
NiII	1454	1454.842	3.23×10^{-2}	-60	100	14.43 ± 0.05	Y	
NiII	1703	1703.405	6.00×10^{-3}	-60	90	14.48 ± 0.07	Y	
NiII	1709	1709.604	3.24×10^{-2}	-60	90	14.44 ± 0.05	Y	
NiII	1741	1741.553	4.27×10^{-2}	-60	90	14.48 ± 0.05	Y	
NiII	1751	1751.916	2.77×10^{-2}	-50	90	14.47 ± 0.05	Y	
NiII	–	–	–	–	–	–	–	14.45 ± 0.05
ZnII	2026	2026.136	4.89×10^{-1}	-60	100	13.57 ± 0.05	Y	
ZnII	–	–	–	–	–	–	–	13.57 ± 0.05

Table A.20: Metal column densities for J1313+1441 ($z_{\text{abs}}=1.79$)

Ion	Line	λ Å	f	v_{min} km s ⁻¹	v_{max} km s ⁻¹	logN(X)	Included	logN _{adopt}
SiII	1304	1304.370	9.40×10^{-2}	-160	195	> 15.29	Y	
SiII	1526	1526.707	1.27×10^{-1}	-160	195	> 15.10	Y	
SiII	1808	1808.013	2.19×10^{-3}	-160	195	16.12 ± 0.05	Y	
SiII	–	–	–	–	–	–	–	16.12 ± 0.05
SII	1250	1250.584	5.43×10^{-3}	-160	195	> 15.75	Y	
SII	1253	1253.811	1.09×10^{-2}	-160	195	> 15.85	N	
SII	–	–	–	–	–	–	–	> 15.75
CrII	2056	2056.254	1.05×10^{-1}	-160	195	13.60 ± 0.05	Y	
CrII	2066	2066.161	5.15×10^{-2}	-160	195	13.65 ± 0.06	Y	
CrII	–	–	–	–	–	–	–	13.61 ± 0.05
FeII	1608	1608.451	5.80×10^{-2}	-160	195	> 15.20	N	
FeII	1611	1611.200	1.36×10^{-3}	-160	195	15.55 ± 0.05	Y	
FeII	–	–	–	–	–	–	–	15.55 ± 0.05
NiII	1317	1317.217	5.71×10^{-2}	-160	195	14.30 ± 0.05	Y	
NiII	1370	1370.131	5.88×10^{-2}	-100	195	14.26 ± 0.05	Y	
NiII	1454	1454.842	3.23×10^{-2}	-160	195	14.09 ± 0.05	Y	
NiII	1709	1709.604	3.24×10^{-2}	-160	195	14.26 ± 0.05	Y	
NiII	1741	1741.553	4.27×10^{-2}	-160	195	14.29 ± 0.05	Y	
NiII	1751	1751.916	2.77×10^{-2}	-160	195	14.37 ± 0.05	Y	
NiII	–	–	–	–	–	–	–	14.27 ± 0.05
ZnII	2026	2026.136	4.89×10^{-1}	-160	195	13.30 ± 0.05	Y	
ZnII	–	–	–	–	–	–	–	13.30 ± 0.05

Table A.21: Metal column densities for J1335+0824 ($z_{\text{abs}}=1.86$)

Ion	Line	λ Å	f	v_{min} km s ⁻¹	v_{max} km s ⁻¹	logN(X)	Included	logN _{adopt}
SiII	1304	1304.370	9.40×10^{-2}	-170	170	> 15.23	N	
SiII	1526	1526.707	1.27×10^{-1}	-170	170	> 15.05	N	
SiII	1808	1808.013	2.19×10^{-3}	-120	130	15.73 ± 0.05	Y	
SiII	–	–	–	–	–	–	–	15.73 ± 0.05
SII	1250	1250.584	5.43×10^{-3}	-120	130	15.26 ± 0.05	Y	
SII	1253	1253.811	1.09×10^{-2}	-120	130	15.30 ± 0.05	Y	
SII	–	–	–	–	–	–	–	15.29 ± 0.05
MnII	1197	1197.184	1.57×10^{-1}	-120	130	13.70 ± 0.10	Y	
MnII	–	–	–	–	–	–	–	13.70 ± 0.10
CrII	2056	2056.254	1.05×10^{-1}	-120	75	13.81 ± 0.05	Y	
CrII	–	–	–	–	–	–	–	13.81 ± 0.05
FeII	1608	1608.451	5.80×10^{-2}	-170	170	> 15.17	Y	
FeII	–	–	–	–	–	–	–	> 15.17
NiII	1317	1317.217	5.71×10^{-2}	-120	130	> 14.26	Y	
NiII	1741	1741.553	4.27×10^{-2}	-120	130	14.29 ± 0.05	Y	
NiII	–	–	–	–	–	–	–	14.29 ± 0.05

Table A.22: Metal column densities for J1417+4132 ($z_{\text{abs}}=1.95$)

Ion	Line	λ Å	f	v_{min} km s ⁻¹	v_{max} km s ⁻¹	logN(X)	Included	logN _{adopt}
SiII	1304	1304.370	9.40×10^{-2}	-105	390	> 15.16	Y	
SiII	1526	1526.707	1.27×10^{-1}	-105	390	> 14.96	Y	
SiII	1808	1808.013	2.19×10^{-3}	-105	390	> 16.42	Y	
SiII	–	–	–	–	–	–	–	> 16.42
CrII	2056	2056.254	1.05×10^{-1}	-105	390	14.03 ± 0.05	Y	
CrII	2066	2066.161	5.15×10^{-2}	-45	390	14.08 ± 0.05	Y	
CrII	–	–	–	–	–	–	–	14.04 ± 0.05
FeII	1608	1608.451	5.80×10^{-2}	-105	390	> 15.22	N	
FeII	1611	1611.200	1.36×10^{-3}	-105	390	15.58 ± 0.05	Y	
FeII	–	–	–	–	–	–	–	15.58 ± 0.05
NiII	1317	1317.217	5.71×10^{-2}	-105	390	14.62 ± 0.05	Y	
NiII	1370	1370.131	5.88×10^{-2}	-105	390	14.58 ± 0.05	Y	
NiII	1454	1454.842	3.23×10^{-2}	-105	150	14.46 ± 0.05	Y	
NiII	1467a	1467.259	6.30×10^{-3}	-30	50	13.92 ± 0.11	N	
NiII	1703	1703.405	6.00×10^{-3}	-105	100	14.36 ± 0.05	Y	
NiII	1709	1709.604	3.24×10^{-2}	-105	250	14.56 ± 0.05	Y	
NiII	1741	1741.553	4.27×10^{-2}	-105	390	14.52 ± 0.05	Y	
NiII	1751	1751.916	2.77×10^{-2}	-105	390	14.53 ± 0.05	Y	
NiII	–	–	–	–	–	–	–	14.55 ± 0.05
ZnII	2026	2026.136	4.89×10^{-1}	-105	390	13.55 ± 0.05	Y	
ZnII	–	–	–	–	–	–	–	13.55 ± 0.05

Table A.23: Metal column densities for J1454+0941 ($z_{\text{abs}}=1.79$)

Ion	Line	λ Å	f	v_{min} km s ⁻¹	v_{max} km s ⁻¹	logN(X)	Included	logN _{adopt}
SiII	1304	1304.370	9.40×10^{-2}	-180	230	> 15.10	N	
SiII	1526	1526.707	1.27×10^{-1}	-180	230	> 14.98	N	
SiII	1808	1808.013	2.19×10^{-3}	-80	70	15.47 ± 0.05	Y	
SiII	–	–	–	–	–	–	–	15.47 ± 0.05
SII	1250	1250.584	5.43×10^{-3}	-80	70	15.25 ± 0.06	Y	
SII	1253	1253.811	1.09×10^{-2}	-80	70	> 15.35	Y	
SII	–	–	–	–	–	–	–	15.25 ± 0.06
CrII	2056	2056.254	1.05×10^{-1}	-80	70	13.30 ± 0.09	Y	
CrII	–	–	–	–	–	–	–	13.30 ± 0.09
FeII	1143	1143.226	1.77×10^{-2}	-80	70	> 15.26	Y	
FeII	1608	1608.451	5.80×10^{-2}	-180	230	> 14.99	N	
FeII	1611	1611.200	1.36×10^{-3}	-80	70	15.02 ± 0.12	Y	
FeII	–	–	–	–	–	–	–	15.02 ± 0.12
NiII	1454	1454.842	3.23×10^{-2}	-80	70	13.86 ± 0.14	Y	
NiII	1709	1709.604	3.24×10^{-2}	-80	70	13.80 ± 0.08	Y	
NiII	1741	1741.553	4.27×10^{-2}	-80	70	13.85 ± 0.05	Y	
NiII	1751	1751.916	2.77×10^{-2}	-80	70	13.90 ± 0.08	Y	
NiII	–	–	–	–	–	–	–	13.85 ± 0.05
ZnII	2026	2026.136	4.89×10^{-1}	-80	70	12.68 ± 0.06	Y	
ZnII	2062	2062.664	2.56×10^{-1}	-80	70	12.87 ± 0.09	Y	
ZnII	–	–	–	–	–	–	–	12.72 ± 0.05

Table A.24: Metal column densities for J1509+1113 ($z_{\text{abs}}=2.03$)

Ion	Line	λ Å	f	v_{min} km s ⁻¹	v_{max} km s ⁻¹	logN(X)	Included	logN _{adopt}
SiII	1304	1304.370	9.40×10^{-2}	-260	160	> 15.14	Y	
SiII	1526	1526.707	1.27×10^{-1}	-260	160	> 14.94	Y	
SiII	1808	1808.013	2.19×10^{-3}	-260	160	16.04 ± 0.05	Y	
SiII	–	–	–	–	–	–	–	16.04 ± 0.05
SiII	1250	1250.584	5.43×10^{-3}	-150	70	15.81 ± 0.05	Y	
SiII	1253	1253.811	1.09×10^{-2}	-150	70	15.60 ± 0.05	Y	
SiII	–	–	–	–	–	–	–	15.69 ± 0.05
FeII	1608	1608.451	5.80×10^{-2}	-120	160	> 15.16	N	
FeII	1611	1611.200	1.36×10^{-3}	-150	70	15.48 ± 0.07	Y	
FeII	–	–	–	–	–	–	–	15.48 ± 0.07
NiII	1317	1317.217	5.71×10^{-2}	-150	70	14.27 ± 0.05	Y	
NiII	1709	1709.604	3.24×10^{-2}	-150	70	14.46 ± 0.06	Y	
NiII	1741	1741.553	4.27×10^{-2}	-150	70	14.41 ± 0.05	Y	
NiII	1751	1751.916	2.77×10^{-2}	-150	70	14.55 ± 0.05	Y	
NiII	–	–	–	–	–	–	–	14.41 ± 0.05

Table A.26: Metal column densities for J1552+4910 ($z_{\text{abs}}=1.96$)

Ion	Line	λ Å	f	v_{min} km s ⁻¹	v_{max} km s ⁻¹	logN(X)	Included	logN _{adopt}
SiII	1526	1526.707	1.27×10^{-1}	-135	120	> 14.96	N	
SiII	1808	1808.013	2.19×10^{-3}	-135	120	15.98 ± 0.05	Y	
SiII	–	–	–	–	–	–	–	15.98 ± 0.05
SiII	1250	1250.584	5.43×10^{-3}	-135	120	15.37 ± 0.05	Y	
SiII	1259	1259.519	1.66×10^{-2}	-135	70	15.34 ± 0.05	Y	
SiII	–	–	–	–	–	–	–	15.34 ± 0.05
MnII	1197	1197.184	1.57×10^{-1}	-135	50	13.39 ± 0.05	Y	
MnII	–	–	–	–	–	–	–	13.39 ± 0.05
CrII	2056	2056.254	1.05×10^{-1}	-135	120	13.79 ± 0.05	Y	
CrII	2066	2066.161	5.15×10^{-2}	-135	120	13.59 ± 0.05	Y	
CrII	–	–	–	–	–	–	–	13.74 ± 0.05
FeII	1142	1142.366	4.20×10^{-3}	-135	120	15.50 ± 0.05	Y	
FeII	1608	1608.451	5.80×10^{-2}	-135	120	> 15.16	N	
FeII	1611	1611.200	1.36×10^{-3}	-135	120	15.43 ± 0.05	Y	
FeII	–	–	–	–	–	–	–	15.47 ± 0.05
NiII	1317	1317.217	5.71×10^{-2}	-135	120	14.27 ± 0.05	Y	
NiII	1370	1370.131	5.88×10^{-2}	-135	120	14.23 ± 0.05	Y	
NiII	1454	1454.842	3.23×10^{-2}	-135	120	14.18 ± 0.05	Y	
NiII	1703	1703.405	6.00×10^{-3}	-135	120	14.41 ± 0.06	Y	
NiII	1709	1709.604	3.24×10^{-2}	-135	120	14.26 ± 0.05	Y	
NiII	1741	1741.553	4.27×10^{-2}	-135	120	14.24 ± 0.05	Y	
NiII	1751	1751.916	2.77×10^{-2}	-135	120	14.28 ± 0.05	Y	
NiII	–	–	–	–	–	–	–	14.24 ± 0.05
ZnII	2026	2026.136	4.89×10^{-1}	-135	120	12.93 ± 0.05	Y	
ZnII	–	–	–	–	–	–	–	12.93 ± 0.05

Table A.28: Metal column densities for J1610+4724 ($z_{\text{abs}}=2.51$)

Ion	Line	λ Å	f	v_{min} km s ⁻¹	v_{max} km s ⁻¹	logN(X)	Included	logN _{adopt}
SiII	1304	1304.370	9.40×10^{-2}	-180	380	> 15.42	Y	
SiII	1526	1526.707	1.27×10^{-1}	-145	380	> 15.22	Y	
SiII	1808	1808.013	2.19×10^{-3}	-180	380	16.16 ± 0.05	Y	
SiII	–	–	–	–	–	–	–	16.16 ± 0.05
CrII	2056	2056.254	1.05×10^{-1}	-70	180	13.91 ± 0.05	Y	
CrII	–	–	–	–	–	–	–	13.91 ± 0.05
FeII	1608	1608.451	5.80×10^{-2}	-180	320	> 15.33	N	
FeII	1611	1611.200	1.36×10^{-3}	-120	140	15.78 ± 0.05	Y	
FeII	2249	2249.877	1.82×10^{-3}	-70	120	15.59 ± 0.05	Y	
FeII	2260	2260.780	2.44×10^{-3}	-70	120	15.61 ± 0.05	Y	
FeII	–	–	–	–	–	–	–	15.62 ± 0.05
NiII	1703	1703.405	6.00×10^{-3}	-50	140	14.48 ± 0.09	Y	
NiII	1709	1709.604	3.24×10^{-2}	-50	140	14.61 ± 0.05	Y	
NiII	1741	1741.553	4.27×10^{-2}	-50	140	14.54 ± 0.05	Y	
NiII	1751	1751.916	2.77×10^{-2}	-50	140	14.58 ± 0.05	Y	
NiII	–	–	–	–	–	–	–	14.58 ± 0.05
ZnII	2026	2026.136	4.89×10^{-1}	-70	180	13.56 ± 0.05	Y	
ZnII	–	–	–	–	–	–	–	13.56 ± 0.05

Table A.29: Metal column densities for J1629+0913 ($z_{\text{abs}}=1.90$)

Ion	Line	λ Å	f	v_{min} km s ⁻¹	v_{max} km s ⁻¹	logN(X)	Included	logN _{adopt}
SiII	1304	1304.370	9.40×10^{-2}	-170	400	> 15.38	N	
SiII	1526	1526.707	1.27×10^{-1}	-170	420	> 15.15	N	
SiII	1808	1808.013	2.19×10^{-3}	-170	50	15.32 ± 0.06	Y	
SiII	–	–	–	–	–	–	–	15.32 ± 0.06
SII	1250	1250.584	5.43×10^{-3}	-170	50	15.09 ± 0.05	Y	
SII	1253	1253.811	1.09×10^{-2}	-170	50	15.29 ± 0.05	Y	
SII	–	–	–	–	–	–	–	15.24 ± 0.05
CrII	2056	2056.254	1.05×10^{-1}	-170	50	< 13.21	Y	
CrII	–	–	–	–	–	–	–	< 13.21
FeII	1608	1608.451	5.80×10^{-2}	-170	140	> 14.93	Y	
FeII	1611	1611.200	1.36×10^{-3}	-170	50	< 15.07	Y	
FeII	–	–	–	–	–	–	–	> 14.93
NiII	1317	1317.217	5.71×10^{-2}	-60	50	13.75 ± 0.13	Y	
NiII	1370	1370.131	5.88×10^{-2}	-170	50	> 13.65	Y	
NiII	1741	1741.553	4.27×10^{-2}	-170	50	< 13.98	Y	
NiII	–	–	–	–	–	–	–	13.75 ± 0.13
ZnII	2026	2026.136	4.89×10^{-1}	-30	50	12.68 ± 0.08	Y	
ZnII	–	–	–	–	–	–	–	12.68 ± 0.08

Table A.30: Metal column densities for Q1755+578 ($z_{\text{abs}}=1.97$)

Ion	Line	λ Å	f	v_{min} km s ⁻¹	v_{max} km s ⁻¹	logN(X)	Included	logN _{adopt}
SiII	1304	1304.370	9.40×10^{-2}	-30	500	> 15.57	Y	
SiII	1526	1526.707	1.27×10^{-1}	-200	500	> 15.43	Y	
SiII	1808	1808.013	2.19×10^{-3}	-200	500	16.58 ± 0.05	Y	
SiII	–	–	–	–	–	–	–	16.58 ± 0.05
SII	1253	1253.811	1.09×10^{-2}	-50	500	> 16.12	Y	
SII	–	–	–	–	–	–	–	> 16.12
MnII	2594	2594.499	2.71×10^{-1}	-200	500	13.80 ± 0.05	Y	
MnII	2606	2606.462	1.93×10^{-1}	-200	500	13.86 ± 0.05	Y	
MnII	–	–	–	–	–	–	–	13.83 ± 0.05
CrII	2056	2056.254	1.05×10^{-1}	-50	500	14.07 ± 0.05	Y	
CrII	2066	2066.161	5.15×10^{-2}	-50	500	14.12 ± 0.05	Y	
CrII	–	–	–	–	–	–	–	14.09 ± 0.05
FeII	1608	1608.451	5.80×10^{-2}	-200	500	> 15.55	Y	
FeII	1611	1611.200	1.36×10^{-3}	-50	500	15.75 ± 0.05	Y	
FeII	2249	2249.877	1.82×10^{-3}	-200	500	15.85 ± 0.05	Y	
FeII	2260	2260.780	2.44×10^{-3}	-200	500	15.81 ± 0.05	Y	
FeII	2344	2344.214	1.14×10^{-1}	-200	500	> 15.22	Y	
FeII	2382	2382.765	3.20×10^{-1}	-200	500	> 14.82	Y	
FeII	2600	2600.173	2.39×10^{-1}	-200	500	> 14.89	Y	
FeII	–	–	–	–	–	–	–	15.79 ± 0.05
NiII	1317	1317.217	5.71×10^{-2}	-50	500	14.77 ± 0.05	Y	
NiII	1370	1370.131	5.88×10^{-2}	-200	500	14.79 ± 0.05	Y	
NiII	1454	1454.842	3.23×10^{-2}	-200	500	14.67 ± 0.05	Y	
NiII	1703	1703.405	6.00×10^{-3}	-200	500	14.84 ± 0.05	Y	
NiII	1709	1709.604	3.24×10^{-2}	-200	500	14.71 ± 0.05	Y	
NiII	1741	1741.553	4.27×10^{-2}	-200	500	14.77 ± 0.05	Y	
NiII	1751	1751.916	2.77×10^{-2}	-200	500	14.76 ± 0.05	Y	
NiII	–	–	–	–	–	–	–	14.75 ± 0.05
ZnII	2026	2026.136	4.89×10^{-1}	0	0	13.85 ± 0.05	Y	
ZnII	–	–	–	–	–	–	–	13.85 ± 0.05

Table A.31: Metal column densities for J2241+1225 ($z_{\text{abs}}=2.42$)

Ion	Line	λ Å	f	v_{min} km s ⁻¹	v_{max} km s ⁻¹	logN(X)	Included	logN _{adopt}
SiII	1304	1304.370	9.40×10^{-2}	-100	25	> 14.67	Y	
SiII	1526	1526.707	1.27×10^{-1}	-90	25	> 14.49	Y	
SiII	–	–	–	–	–	–	–	> 14.67
SII	1253	1253.811	1.09×10^{-2}	-100	25	> 15.01	Y	
SII	1259	1259.519	1.66×10^{-2}	-100	25	> 14.91	Y	
SII	–	–	–	–	–	–	–	> 15.01
MnII	1197	1197.184	1.57×10^{-1}	-100	25	13.36 ± 0.13	Y	
MnII	–	–	–	–	–	–	–	13.36 ± 0.13
FeII	1081	1081.875	1.40×10^{-2}	-100	25	> 15.02	Y	
FeII	1142	1142.366	4.20×10^{-3}	-100	25	15.01 ± 0.08	Y	
FeII	1608	1608.451	5.80×10^{-2}	-100	25	> 14.45	N	
FeII	1611	1611.200	1.36×10^{-3}	-100	25	< 15.12	Y	
FeII	–	–	–	–	–	–	–	15.02 ± 0.08
NiII	1317	1317.217	5.71×10^{-2}	-100	25	13.89 ± 0.05	Y	
NiII	1370	1370.131	5.88×10^{-2}	-100	25	13.65 ± 0.10	Y	
NiII	–	–	–	–	–	–	–	13.83 ± 0.05